area under the curve while reducing the peak plasma DNP concentrations with a sustained-release coating increased the ratio of toxic to effective dose 25-fold over liver-targeted DNP and 1250-fold over unaltered DNP. These data support the potential utility of mitochondrial protonophores and other mitochondrial uncoupling agents for the treatment of the related epidemics of NASH, metabolic syndrome, and T2D.

REFERENCES AND NOTES

1. V. Ratziu, S. Bellentani, H. Cortez-Pinto, C. Day, G. Marchesini, *J. Hepatol.* **53**, 372–384 (2010).
2. V. T. Samuel *et al.*, *J. Biol. Chem.* **279**, 32345–32353 (2004).
3. R. J. Perry *et al.*, *Cell Metab.* **18**, 740–748 (2013).
4. R. J. Perry *et al.*, *Nat. Med.* **20**, 759–763 (2014).
5. I. A. Leclercq *et al.*, *J. Clin. Invest.* **105**, 1067–1075 (2000).
6. E. Ip, G. Farrell, P. Hall, G. Robertson, I. Leclercq, *Hepatology* **39**, 1286–1296 (2004).
7. K. F. Petersen *et al.*, *Am. J. Physiol.* **276**, E529–E535 (1999).

ACKNOWLEDGMENTS

We thank J. Dong, C. Soroka, J. P. Camporez, M. Jurczak, J. Stack, M. Kahn, C. Borders, Y. Kosover, A. Nasiri, G. Butrico, M. Batsu, and W. Zhu for their invaluable technical assistance; C. Frassetto and A. Barkley for their work to formulate the CRMP; B. Ehrlich for assistance with the thermal algesia studies; M. Kashgarian for expert analysis of renal histology; and A. Ray and C. Tay for toxicology advice. Yale University has applied for a patent (provisional patent application 61/919, 003) related to the use of CRMP and similar protonophores for the treatment of metabolic diseases, including NAFLD/NASH and T2D. This research was funded by grants from the United States National Institutes of Health (R01 DK-40936, R24 DK-085638, U24 DK-059635, T32 DK-101019, P30 DK-45735, P30 DK-34989, and UL1 TR-000142) and the Novo Nordisk Foundation Center for Basic Metabolic Research, University of Copenhagen, Copenhagen, Denmark.

SUPPLEMENTARY MATERIALS

www.sciencemag.org/content/347/6227/1253/suppl/DC1
Materials and Methods
Figs. S1 to S13
References (*8*–*17*)

11 October 2014; accepted 5 February 2015
Published online 26 February 2015;
10.1126/science.aaa0672

ION CHANNELS

K2P channel gating mechanisms revealed by structures of TREK-2 and a complex with Prozac

Yin Yao Dong,[1]* Ashley C. W. Pike,[1]* Alexandra Mackenzie,[1,2] Conor McClenaghan,[2,3] Prafulla Aryal,[2,3,4] Liang Dong,[1]† Andrew Quigley,[1] Mariana Grieben,[1] Solenne Goubin,[1]‡ Shubhashish Mukhopadhyay,[1] Gian Filippo Ruda,[1,5] Michael V. Clausen,[2] Lishuang Cao,[6] Paul E. Brennan,[1,5] Nicola A. Burgess-Brown,[1] Mark S. P. Sansom,[3,4] Stephen J. Tucker,[2,3]§ Elisabeth P. Carpenter[1,3]§

TREK-2 (KCNK10/K2P10), a two-pore domain potassium (K2P) channel, is gated by multiple stimuli such as stretch, fatty acids, and pH and by several drugs. However, the mechanisms that control channel gating are unclear. Here we present crystal structures of the human TREK-2 channel (up to 3.4 angstrom resolution) in two conformations and in complex with norfluoxetine, the active metabolite of fluoxetine (Prozac) and a state-dependent blocker of TREK channels. Norfluoxetine binds within intramembrane fenestrations found in only one of these two conformations. Channel activation by arachidonic acid and mechanical stretch involves conversion between these states through movement of the pore-lining helices. These results provide an explanation for TREK channel mechanosensitivity, regulation by diverse stimuli, and possible off-target effects of the serotonin reuptake inhibitor Prozac.

Two-pore domain potassium (K2P) channels contribute to the background leak potassium currents in nearly all cells and exhibit versatile, polymodal patterns of regulation. This functional diversity contributes to regulation of the resting membrane potential in many excitable and nonexcitable tissues. K2P channels represent important clinical targets for the treatment of cardiovascular disease and several neurological disorders, including pain and depression (*1*).

The archetypal polymodal K2P channels TREK-1 and TREK-2 are regulated by physical factors such as mechanical stretch, voltage, and temperature; by natural ligands including polyunsaturated fatty acids such as arachidonic acid (AA); and by intra- and extracellular pH (pH_{int} and pH_{ext}) (*1*–*3*). Their activity can also be modulated by diverse pharmacological agents such as volatile anesthetics, neuroprotective drugs, and antidepressants such as fluoxetine (Prozac) (*1*–*6*). Such diverse regulation allows these channels to couple cellular electrical activity to a variety of signaling pathways; consequently, they represent important pharmacological targets (*6*). In particular, TREK channels are inhibited in vitro by fluoxetine and its active metabolite norfluoxetine at physiologically relevant concentrations (*4*, *5*, *7*). This selective serotonin reuptake inhibitor is used in the treatment of a range of depressive and anxiety disorders. In addition to its principal effect of directly inhibiting serotonin transporters, fluoxetine also inhibits several G protein–coupled receptors and ion channels (*4*, *8*). TREK-1 knockout mice appear resistant to depression, suggesting that TREK channel inhibition by fluoxetine may contribute to its antidepressant effects (*5*, *8*). Inhibition of TREK channels in the cardiovascular system may also contribute to some of the drug's known side effects (*9*). Norfluoxetine is a state-dependent blocker of TREK channels (*4*) and is used here as a tool compound to probe the structural basis of TREK channel inhibition.

The molecular and structural mechanisms that allow K2P channels to sense such diverse stimuli are poorly understood. Structures of two members of the K2P channel family (TRAAK and TWIK-1) reveal that they share many basic structural features with classical tetrameric K^+ channels but assemble as dimers with a pseudotetrameric pore (*10*–*12*). Also, they do not appear to gate via constriction of the cytoplasmic entrance to the pore. Instead, this lower part of the conduction pathway remains open even when the channel is closed, and gating occurs primarily within the selectivity filter (*2*, *13*, *14*). However, the mechanisms that relay regulatory stimuli to the pore, and how drugs modulate this process, remain unclear.

To understand the mechanisms of polymodal K2P channel gating and inhibition by drugs, we solved the crystal structure of human TREK-2 in two conformations at 3.4 and 3.9 Å resolution (*15*) (figs. S1 and S2 and table S1). The truncated protein used for crystallization retains many functional properties exhibited by wild-type TREK-2, including activation by stretch and AA and inhibition by norfluoxetine (fig. S3). The two TREK-2 structures show the classic K2P channel fold (*10*–*12*), with four transmembrane helices (M1 to M4), two pore-forming regions per chain (P1 and P2), and an extracellular cap domain (Fig. 1, A and B). TREK-2 exhibits the domain swap seen in TRAAK (*10*) (fig. S4).

Differences between the two conformations are centered around the lower sections of the M2, M3, and M4 helices (Fig. 1, C and D; fig. S5; and movie S1). In the 3.9 Å structure, these

[1]Structural Genomics Consortium, University of Oxford, Oxford OX3 7DQ, UK. [2]Clarendon Laboratory, Department of Physics, University of Oxford, Oxford OX1 3PU, UK. [3]OXION Initiative in Ion Channels and Disease, University of Oxford, Oxford OX1 3PN, UK. [4]Department of Biochemistry, University of Oxford, Oxford OX1 3QU, UK. [5]Target Discovery Institute, Nuffield Department of Medicine, University of Oxford, Oxford OX3 7FZ, UK. [6]Pfizer Neusentis, Granta Park, Cambridge CB21 6GS, UK.
*These authors contributed equally to this work. †Present address: Department of Clinical Neurosciences, Cambridge Institute for Medical Research, University of Cambridge, Cambridge CB2 0XY, UK. ‡Present address: Solenne Goubin, School of Veterinary Medicine and Science, University of Nottingham, Sutton Bonington Campus, Sutton Bonington, Leicestershire LE12 5RD, UK.
§Corresponding author. E-mail: liz.carpenter@sgc.ox.ac.uk (E.P.C.); stephen.tucker@physics.ox.ac.uk (S.J.T.)

regions project further into the cytoplasm (the "down state"), whereas in the 3.4 Å structure, they move further up into the membrane (the "up state"). In both structures there are two copies of the dimer in the asymmetric unit, and each of the four chains adopts a similar conformation, despite different crystal-packing arrangements (fig. S6), suggesting that the two conformations are not imposed by crystal packing. Profiles of the inner pore show that the cytoplasmic entrance to the vestibule remains open in both conformations (Fig. 1D and fig. S5, D to F). In the up state, M4 is kinked, with a hinge around a conserved glycine (Gly^{312}). In addition, there are hinges in M2 at Gly^{201}/Gly^{206}

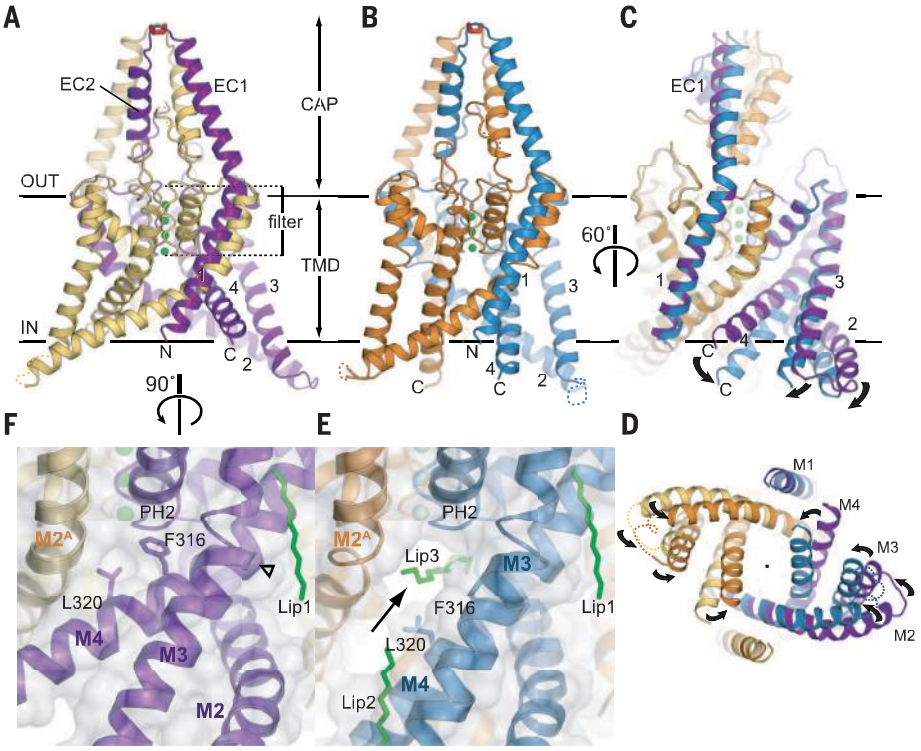

Fig. 1. Crystal structures of two conformations of TREK-2. TREK-2 overall fold viewed parallel to the plane of the membrane, with views of (**A**) the up-state 3.4 Å structure, with chains A and B in yellow and purple; (**B**) the down-state 3.9 Å structure, with chains A and B in orange and blue; (**C**) a superposition of the states; and (**D**) the superposition viewed from the cytoplasmic side of the membrane. Potassium ions are colored green and the cap disulfide bond in red. (**E**) Fenestration (indicated with an arrow) in the down state, with the aliphatic chain that binds in the vestibule and the fenestration (Lip3) and lipids (Lip1, Lip2) on the channel surface (green sticks). (**F**) View of the up state, in the same orientation as in (E), showing absence of the fenestration due to elevation of M4 and insertion of the side chains of Phe^{316} and Leu^{320} into the fenestration. The hinge point around Gly^{312} in M4 is indicated by an open triangle. N, N terminus; C, C terminus; CAP, extracellular CAP domain; TMD. transmembrane domain.

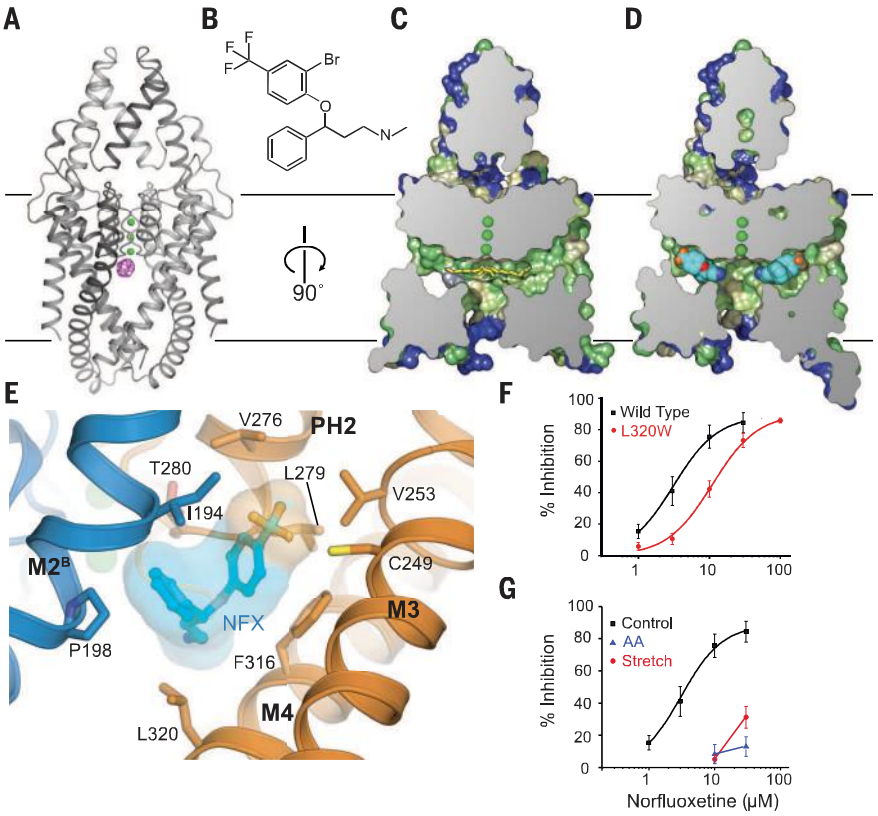

Fig. 2. Norfluoxetine and Br-fluoxetine bind to TREK-2 in the down-state fenestration adjacent to the pore filter entrance. (**A**) Overall fold of the TREK-2 down state shown with the 5 Å anomalous difference map for the Br-fluoxetine/TREK-2 complex shown in pink (contoured at 4.5σ), indicating the location of Br-fluoxetine in the fenestration. (**B**) Chemical structure of Br-fluoxetine. Norfluoxetine lacks the methyl group on the nitrogen. (**C**) Cross section of a surface view of TREK-2 in the down state, colored by hydrophobicity [green (most hydrophobic) through yellow to blue (least hydrophobic)]. Yellow sticks represent Lip3. (**D**) Complex of TREK-2 with norfluoxetine. Norfluoxetine is shown in light blue, dark blue, red, and orange for carbon, nitrogen, oxygen, and fluorine atoms, respectively. For clarity, only one enantiomer of norfluoxetine is shown in (D) and (E). (**E**) Norfluoxetine binding site, with chains A and B in gold and blue, respectively, and norfluoxetine colored as in (D). (**F**) Disruption of the binding site by the L320W mutation reduces norfluoxetine inhibition. (**G**) Stretch activation (–11 mmHg, red) at pH_{int} 7.3 dramatically reduces the efficacy of norfluoxetine inhibition, as does activation by 10 μM AA (blue). Error bars in (F) and (G) denote ± SEM.

and in M3 at Gly[248], allowing movement of all three helices (Fig. 1F). The down state is similar to that previously observed in the K2P channels TRAAK and TWIK-1 (*10*–*12*). We observe substantial movement of all three helices (M2, M3, and M4) between the two conformations (movie S1 and fig. S5). While this manuscript was under review, two studies of TRAAK also observed movement of M4 in both chains (*16*, *17*) or of M2 in one of the chains (*17*), and these movements were associated with the regulation of channel activity. In TREK-2, we observe movement of all three helices (M2, M3, and M4) in both chains. This coordinated movement of all three helices is supported by molecular dynamics (MD) simulations of the structures within a bilayer. These simulations exhibit downward movement of M2, M3, and M4 in the up state to adopt a conformation similar to the down state, thus indicating that movement between states can occur (fig. S7).

A key feature of K2P channel structures is the intramembrane-side fenestrations just below the selectivity filter (*11*, *12*). These are present only in the down state (Fig. 1E). In the up state, the fenestration is closed by the upward movement and rotation of M4, which places the side chains of Phe[316] and Leu[320] in the fenestration (Fig. 1F). In the TREK-2 and TWIK-1 down states, there is density for lipid-like molecules extending across the top of the inner vestibule below the filter (Fig. 1E and fig. S5, A and B), which may represent copurified lipids or polyethylene glycol molecules.

To form a fully conductive channel, all four K^+ binding sites within the filter must be occupied (*18*, *19*). The TREK-2 up state has electron density for four K^+ ions in the filter, suggesting that this state is conductive. By contrast, the down state has density for only three ions (Fig. 1, A and B, and fig. S8), implying that it may represent a nonconductive state, even though the inner pore is open. However, the available TRAAK and TWIK-1 structures (*10*–*12*, *16*, *17*) have similar occupancy for all four sites within the filter in both states.

To probe the functional importance of these two states, we examined TREK-2 inhibition by fluoxetine and norfluoxetine because both exhibit state-dependent inhibition of TREK channel activity via a selective interaction with the closed state (*4*). We solved the structure of TREK-2 in complex with norfluoxetine and brominated fluoxetine {3-[2-bromo-4-(trifluoromethyl) phenoxy]-*N*-methyl-3-phenylpropan-1-amine (hereafter referred to as Br-fluoxetine)} at 3.7 and 3.64 Å resolution (Fig. 2 and fig. S9). These structures were in the down state with clear peaks in anomalous difference maps for bromine in Br-fluoxetine in the fenestrations (Fig. 2A and fig. S9), unequivocally identifying the binding site for Br-fluoxetine. Norfluoxetine was also found bound within the fenestration (Fig. 2, C to E, and movie S1), but neither ligand extended into the vestibule to block the ion path directly (Fig. 2, D and E). The fenestration provides a hydrophobic environment close to the selectivity filter in which both Br-fluoxetine and norfluoxetine interact with residues Ile[194] and Pro[198] on M2 of chain B, Cys[249] and Val[253] on M3, Phe[316] and Leu[320] on M4, and Val[276], Leu[279], and Thr[280] on pore helix 2 (Fig. 2E). There is some flexibility in positioning of fluoxetine derivatives (fig. S9), but this is not

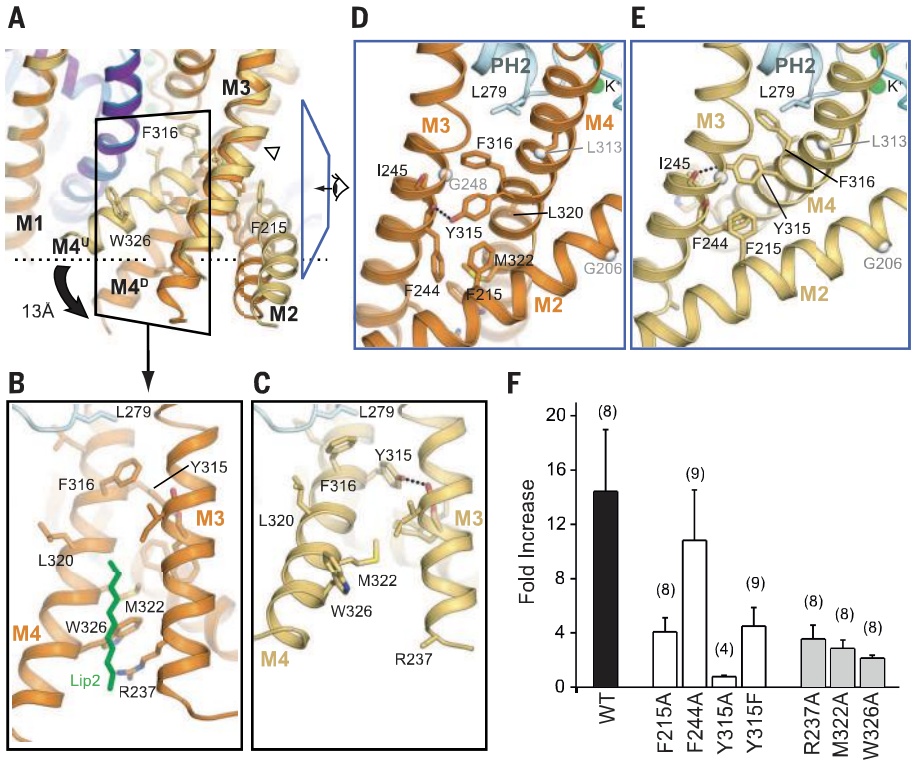

Fig. 3. Concerted motion of transmembrane helices M2, M3, and M4. (**A**) Superposition of the up and down states highlighting movement of M2 to M4. (**B**) Interactions between helices M2, M3, and M4 in the down state, involving Trp[326], Arg[237], and Met[322]. View shown is indicated by black boxed region in (A). The lipid chain that overlays this interface is shown in green. (**C**) View of corresponding region in the up state, showing disruption of the distal M3-M4 interface due to a shift in M4 orientation. (**D** and **E**) Interactions at the top of the M2, M3, and M4 helices, proximal to the pore in the down (D) and up (E) states viewed from the direction indicated by blue boxed region in (A). Transmembrane helix hinge points are indicated by gray spheres. (**F**) Mutations at the interface between M2, M3, and M4 reduce activation by membrane stretch (–11 mmHg). Error bars denote ± SEM; numbers in parentheses indicate the number of repeats. WT, wild type.

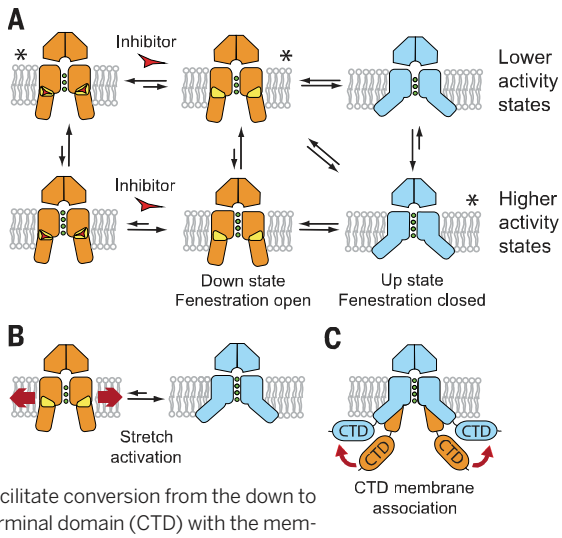

Fig. 4. Model of K2P channel gating and inhibition by norfluoxetine. The down state is shown in orange, fenestrations in yellow, and the up state in blue. Inhibitors such as norfluoxetine are represented by a red triangle-like symbol. (**A**) Overall scheme for K2P channel gating. Higher- and lower-activity states are shown for both conformations, as the filter may gate independently of these larger changes, though with a different probability. Conformations seen in crystal structures are indicated by asterisks. (**B**) Schematic of activation of TREK channels by mechanical stretch. The direct interaction of TREK-2 with lipids in the membrane may allow lateral forces to facilitate conversion from the down to the up state. (**C**) Association of the C-terminal domain (CTD) with the membrane. The diverse cytoplasmic C-terminal extensions of K2P channels provide an additional site for modulation of channel activity. Posttranslational modification of the CTD or protonation due to pH changes could favor association of the CTD with the membrane, thus stabilizing the more active up state.

unexpected for a relatively low-affinity ligand. Furthermore, a mutation within the binding site [Leu^{320}→Trp^{320} (L320W) on M4] (*20*) reduces the inhibition of TREK-2 by norfluoxetine (Fig. 2F).

The fenestration is present only in the down state; transition to the up state closes the fenestration, thus removing the norfluoxetine binding site. This is consistent with a state-dependent block of the closed channel by norfluoxetine (*4*) and with the observation that in the down state there are only three K^+ ions in the filter, suggesting a nonconductive state. It also predicts that the up state represents a more activated state, which does not bind norfluoxetine. To test this hypothesis, we examined the effect of channel activation on norfluoxetine inhibition. We found that activation either by membrane stretch or AA reduced subsequent norfluoxetine inhibition (Fig. 2G). The mechanisms underlying both stretch and AA activation are thought to be similar (*21*, *22*), suggesting that the up state may represent a conformation activated by stretch and AA. Furthermore, we found that norfluoxetine markedly slows the rate of stretch activation (fig. S10A). These effects are consistent with fluoxetine preventing conversion between the two states. In addition, norfluoxetine's binding site close to the filter gate may also help to stabilize the nonconductive state.

Movement between these two conformations provides a structural mechanism for coupling regulatory signals to the filter gate. In particular, it allows movement of M4 to be coupled to the cytoplasmic domain, which moves on and off the membrane surface in response to various regulatory signals (*8*, *13*, *21*, *23*). Movement of the helices between states is also associated with reorientation of side chains between M2, M3, and M4. At the cytoplasmic end of M4, Trp^{326} is packed between the side chains of Met^{322} on M4 and Arg^{237} on M3 in the down state (Fig. 3, A and B). However, in the up state, a kinking and 30° rotation of M4 allows the Trp^{326} side chain to insert into the bilayer, moving the three helices further into the membrane (Fig. 3, A and C). Disruption of these interactions should therefore preferentially destabilize the down state, and we found that mutation of these residues (W326A, M322A, and R237A) reduced stretch activation. (Fig. 3F and fig. S10C).

Immediately above Trp^{326}, a set of hydrophobic residues (Phe^{215}, Phe^{244}, Ile^{245}, and Tyr^{315}) form another core of interactions between M2, M3, and M4 (Fig. 3, D and E). These side chains all rearrange between conformations (Fig. 3A). Mutations within this region also reduced stretch activation (Fig. 3F and fig. S10C). In particular, Tyr^{315} on M4 hydrogen bonds with the backbone carbonyl of Phe^{244} on M3 in the up state but shifts to Ile^{245} in the down state. Both the Y315A and Y315F mutations reduced stretch activation, supporting a functional role for this interaction (Fig. 3, D and E).

TREK channels are regulated by many natural lipids in addition to AA (*24*). We observe lipid-like density on the channel surface in grooves at the top and bottom of M3 and M4: The lower site is found only in the down state, packed against Trp^{326}, potentially stabilizing the down state, whereas the upper site is found in both conformations (Fig. 3B). MD simulations confirm that both of these sites can accommodate lipids (fig. S11).

TREK-2 is also sensitive to changes in both intracellular and extracellular pH. Lower external pH (pH_{ext}) affects the filter gate through protonation of a conserved histidine (His^{156}) and also the external P2-M4 linker (*25*). Our structures reveal that His^{156} is located within a solvent-accessible extracellular cavity adjacent to both the P1-M2 and P2-M4 linkers (fig. S12, A to C). It is also at the center of an extensive hydrogen bond network. Mutations within either this network or the linkers affected the response to pH_{ext} (fig. S12D), which suggests that the structural dynamics of this network may couple external stimuli to the filter gate. Intracellular acidification (pH_{int}) also activates TREK-2, and a glutamate residue within the proximal C terminus (Glu^{337}) is critical for this process (*21*). However, this region is not resolved in our structures. Furthermore, pH_{int} activation does not reduce norfluoxetine inhibition (fig. S10B), suggesting that the mechanism underlying pH_{int} activation may be different from that of stretch and AA activation. Nevertheless, this distal segment of M4 is still well positioned to affect movement between the up and down states, thereby integrating many regulatory pathways (*8*, *21*).

These studies allow us to propose a gating mechanism (Fig. 4) in which movement of the pore-lining helices converts TREK-2 between two functional states. The down state represents a closed or "low-activity" state stabilized by inhibitors such as norfluoxetine binding within the fenestrations. By contrast, activation by membrane stretch or AA stabilizes a "higher-activity" up state that is insensitive to norfluoxetine (Fig. 4). It is possible that these two conformations represent the only open and closed states, but differences in filter-ion occupancy in the down state compared with TRAAK (*16*, *17*) suggest that the filter may be able to gate independently in both conformations, perhaps with a higher open probability in the up state (Fig. 4). Our results provide a mechanism for coupling mechanical forces within the membrane to channel activity through movement of the transmembrane helices (Fig. 4), supporting recent evidence that mechanosensitive K2P channels sense force directly through interactions with lipids (*26*–*28*). A related mechanism of mechanosensitivity has been proposed for the TRAAK channel (*16*), but precisely how such conformational changes influence the selectivity filter gate (*14*, *23*), the relative hydration status of the inner pore (*29*), and whether physiological lipids can sterically occlude the pore in the down state (*30*) remain to be determined. Nevertheless, our results clearly demonstrate how movement of the pore-lining helices creates a mechanism for regulation of K2P channel gating by diverse stimuli and illustrate how state-dependent inhibition of TREK channels by Prozac may contribute to possible off-target effects of the drug.

REFERENCES AND NOTES

1. P. Enyedi, G. Czirják, *Physiol. Rev.* **90**, 559–605 (2010).
2. A. Cohen, Y. Ben-Abu, N. Zilberberg, *Eur. Biophys. J.* **39**, 61–73 (2009).
3. J. Noël, G. Sandoz, F. Lesage, *Channels* **5**, 402–409 (2011).
4. L. E. Kennard *et al*., *Br. J. Pharmacol.* **144**, 821–829 (2005).
5. C. Heurteaux *et al*., *Nat. Neurosci.* **9**, 1134–1141 (2006).
6. Z. Es-Salah-Lamoureux, D. F. Steele, D. Fedida, *Trends Pharmacol. Sci.* **31**, 587–595 (2010).
7. M. E. Henry *et al*., *Neuropsychopharmacology* **30**, 1576–1583 (2005).
8. E. Honoré, *Nat. Rev. Neurosci.* **8**, 251–261 (2007).
9. A. Gurney, B. Manoury, *Eur. Biophys. J.* **38**, 305–318 (2009).
10. S. G. Brohawn, E. B. Campbell, R. MacKinnon, *Proc. Natl. Acad. Sci. U.S.A.* **110**, 2129–2134 (2013).
11. S. G. Brohawn, J. del Mármol, R. MacKinnon, *Science* **335**, 436–441 (2012).
12. A. N. Miller, S. B. Long, *Science* **335**, 432–436 (2012).
13. S. N. Bagriantsev, R. Peyronnet, K. A. Clark, E. Honoré, D. L. Minor Jr., *EMBO J.* **30**, 3594–3606 (2011).
14. P. L. Piechotta *et al*., *EMBO J.* **30**, 3607–3619 (2011).
15. Materials and methods are available as supplementary materials on *Science* Online.
16. S. G. Brohawn, E. B. Campbell, R. MacKinnon, *Nature* **516**, 126–130 (2014).
17. M. Lolicato, P. M. Riegelhaupt, C. Arrigoni, K. A. Clark, D. L. Minor Jr., *Neuron* **84**, 1198–1212 (2014).
18. M. Zhou, J. H. Morais-Cabral, S. Mann, R. MacKinnon, *Nature* **411**, 657–661 (2001).
19. D. A. Köpfer *et al*., *Science* **346**, 352–355 (2014).
20. Single-letter abbreviations for the amino acid residues are as follows: A, Ala; C, Cys; D, Asp; E, Glu; F, Phe; G, Gly; H, His; I, Ile; K, Lys; L, Leu; M, Met; N, Asn; P, Pro; Q, Gln; R, Arg; S, Ser; T, Thr; V, Val; W, Trp; and Y, Tyr.
21. E. Honoré, F. Maingret, M. Lazdunski, A. J. Patel, *EMBO J.* **21**, 2968–2976 (2002).
22. F. Maingret, A. J. Patel, F. Lesage, M. Lazdunski, E. Honoré, *J. Biol. Chem.* **274**, 26691–26696 (1999).
23. S. N. Bagriantsev, K. A. Clark, D. L. Minor Jr., *EMBO J.* **31**, 3297–3308 (2012).
24. J. Chemin *et al*., *Pflugers Arch.* **455**, 97–103 (2007).
25. G. Sandoz, D. Douguet, F. Chatelain, M. Lazdunski, F. Lesage, *Proc. Natl. Acad. Sci. U.S.A.* **106**, 14628–14633 (2009).
26. A. Anishkin, S. H. Loukin, J. Teng, C. Kung, *Proc. Natl. Acad. Sci. U.S.A.* **111**, 7898–7905 (2014).
27. S. G. Brohawn, Z. Su, R. MacKinnon, *Proc. Natl. Acad. Sci. U.S.A.* **111**, 3614–3619 (2014).
28. J. Teng, S. Loukin, A. Anishkin, C. Kung, *Pflugers Arch.* **467**, 27–37 (2015).
29. P. Aryal, F. Abd-Wahab, G. Bucci, M. S. Sansom, S. J. Tucker, *Nat. Commun.* **5**, 4377 (2014).
30. P. Aryal, F. Abd-Wahab, G. Bucci, M. S. Sansom, S. J. Tucker, *Channels* **9**, 44–49 (2015).

ACKNOWLEDGMENTS

The Structural Genomics Consortium is a registered charity (no. 1097737) that receives funds from AbbVie, Bayer, Boehringer Ingelheim, Genome Canada through Ontario Genomics Institute grant OGI-055, GlaxoSmithKline, Janssen, Lilly Canada, the Novartis Research Foundation, the Ontario Ministry of Economic Development and Innovation, Pfizer, Takeda, and Wellcome Trust grant 092809/Z/10/Z. M.S.P.S. and S.J.T. are supported by the UK Biotechnology and Biological Sciences Research Council and the Wellcome Trust. Atomic coordinates and structure factors have been deposited with the Protein Data Bank under accession codes 4XDJ (down state), 4BW5 (up state), 4XDL (Br-fluoxetine complex), and 4XDK (norfluoxetine complex). We declare no competing financial interests.

SUPPLEMENTARY MATERIALS

www.sciencemag.org/content/347/6227/1256/suppl/DC1
Materials and Methods
Supplementary Text
Figs. S1 to S13
Table S1
References (*31*–*49*)
Movie S1

22 September 2014; accepted 5 February 2015
10.1126/science.1261512

Supplementary Materials for

K2P channel gating mechanisms revealed by structures of TREK-2 and a complex with Prozac

Yin Yao Dong, Ashley C. W. Pike, Alexandra Mackenzie, Conor McClenaghan, Prafulla Aryal, Liang Dong, Andrew Quigley, Mariana Grieben, Solenne Goubin, Shubhashish Mukhopadhyay, Gian Filippo Ruda, Michael V. Clausen, Lishuang Cao, Paul E. Brennan, Nicola A. Burgess-Brown, Mark S. P. Sansom, Stephen J. Tucker,* Elisabeth P. Carpenter*

*Corresponding author. E-mail: liz.carpenter@sgc.ox.ac.uk (E.P.C.); stephen.tucker@physics.ox.ac.uk (S.J.T.)

Published 13 March 2015, *Science* **347**, 1256 (2015)
DOI: 10.1126/science.1261512

This PDF file includes:

Other Supplementary Material for this manuscript includes the following:
(available at www.sciencemag.org/content/347/6227/1256/suppl/DC1)

Materials and Methods

Cloning and expression

The gene for TREK-2 (KCNK10) was purchased from the Mammalian Gene Collection (MGC:104160, IMAGE: 30915621, BC075021). The construct used for structure determination consisted of residues Gly^{67} to Glu^{340} of TREK-2, with a C-terminal purification tag with a tobacco etch virus (TEV) protease cleavage site, a 10x His purification sequence and a FLAG tag, in the expression vector pFB-CT10HF-LIC (available from the SGC). Baculoviruses were produced by transformation of DH10Bac cells. *Spodoptera frugiperda* (Sf9) insect cells in Sf-900 II SFM medium (Life Technologies) were infected with recombinant baculovirus and incubated for 65 h at 27 °C in shaker flasks.

Purification of TREK-2

Cell pellets from 1 litre of insect cell culture were resuspended in 50 ml of extraction buffer (50 mM HEPES, pH 7.5, 200 mM KCl, 5 mM imidazole, Roche protease inhibitor cocktail) and lysed by two passes through an EmulsiFlex-C5 homogenizer (Aventis). Protein was extracted from cell membranes by incubation of the crude lysate with 1 % (w/v) OGNG and 0.1 % (w/v) CHS for 1 h at 4 ºC. Cell debris and unlysed cells were removed by centrifugation at 35,000 g for 1 h. Detergent-solubilized protein was purified by immobilized metal affinity chromatography by batch binding to Co^{2+} charged TALON resin (Clontech) at 4 ºC for 1 h. The resin was washed with 30 column volumes of wash buffer (50 mM HEPES, pH 7.5, 200 mM KCl, 20 mM imidazole, 0.18 % OGNG and 0.018 % CHS) and eluted with wash buffer supplemented with 250 mM imidazole. The eluted protein was desalted using a PD10 column (GE healthcare) pre-equilibrated with extraction buffer containing 0.18 % OGNG and 0.018 % CHS. Desalted protein was subsequently treated with 10:1 TEV protease and 20:1 PNGaseF (w:w, protein:enzyme) overnight at 4 ºC. The TEV and PNGaseF treated protein was separated from the 6x His-tagged enzymes and uncleaved TREK-2 by incubation for 1h with TALON resin at 4 °C. The resin was collected in a column and the flow-through and initial wash with extraction buffer were collected and concentrated to 0.5 ml using a 30 kDa cut-off concentrator (Corning). The concentrated protein was further purified by size exclusion chromatography (SEC) using a Superose 6 10/300GL column (GE Healthcare) equilibrated with SEC buffer (20 mM HEPES, pH 7.5, 200 mM KCl, 0.12 % OGNG and 0.012 % CHS) (fig. S1). The four peak fractions (0.5 ml fractions) containing the highest protein concentration were combined and concentrated in a 2 ml 30 kDa concentrator (Sartorius) for crystallization (fig. S1B).

Crystallization of TREK-2

Protein was concentrated to 20 mg/ml, then diluted to 9–12 mg/ml using SEC buffer without added detergent. Initial crystals were grown at 4ºC from sitting drops (150-200 nl) set up in 96-well format using a Mosquito crystallization robot (TTP Labtech) and protein:reservoir ratios of 2:1, 1:1 and 1:2. Two crystal forms of TREK-2 were observed depending on the crystallization conditions. Form 1 (up state) crystals were initially obtained in an in-house version of MemGold HT-96 screen (Molecular Dimensions) (*31*) condition H11. Form 1 crystallization conditions were optimized to give a final reservoir

solution containing 31 % (v/v) polyethylene glycol (PEG) 400, 1 mM cadmium chloride, 2 % (w/v) benzamidine, 0.1 M HEPES, pH 8.0. Form 1 crystals were obtained at pHs between 6.5 and 8.0. The highest resolution data were obtained from crystals grown at pH 8.0, but we also obtained data for form 1 crystals grown at pH 6.5. Form 2 (down state) crystals were obtained in MemGold2 (Molecular Dimensions) (*32*) conditions E4 and G11. Optimized crystals were grown from 150 nl drops comprising 90 nl protein solution (12.1 mg/ml) and 60 nl reservoir solution containing 22 % (w/v) PEG1500, 3 % (v/v) methanol, 0.1 M sodium cacodylate, pH 6.5.

Form 1 crystals were cryo-cooled by slow transfer into artificial mother liquor containing 0.2 M potassium chloride, 2 % (w/v) benzamidine, 0.2 % OGNG / 0.02 % CHS, 0.1 M HEPES, pH 8.0, 35 % (v/v) PEG400 followed by plunging into liquid nitrogen. Form 2 crystals were similarly equilibrated against solutions containing increasing concentrations of PEG1500 (22-35 %) prior to cryo-cooling in liquid nitrogen. Diffraction of the form 1 crystals was improved by slowly increasing the concentration of PEG400 to above 35 % (v/v) which resulted in a 10 % shrinkage in unit cell volume compared to untreated crystals.

Racemic Br-fluoxetine synthesis

Racemic 3-(2-bromo-4-(trifluoromethyl)phenoxy)-*N*-methyl-3-phenylpropan-1-amine **3** was prepared following the reported procedure for the synthesis of fluoxetine (*33*), starting from 2-bromo-1-fluoro-4-(trifluoromethyl)benzene **2** and 3-methylamino-1-phenylpropanol **1** (fig. S13). The title compound was converted into its hydrochloride salt by addition of a dry HCl in diethyl ether to a solution of **1** in dry diethyl ether.

LCMS [ES^+]: Rt 7.0; m/z (rel. abundance): 388.02 (95), 389.03 (20), 390.02 (100), 391,02 (25) $[M+H]^+$. ^{1}H NMR (400 MHz, DMSO-d_6) δ 7.93 (1H, d, *J*=1.7 Hz), 7.58 (1H, dd, *J*=1.8, 8.7 Hz), 7.40 - 7.37 (4H, m), 7.31 - 7.26 (1H, m), 7.12 (1H, d, *J*=8.7 Hz), 5.70 (1H, dd, *J*=5.1, 7.9 Hz), 2.62 - 2.49 (2H, m), 2.27 (3H, s), 2.18 - 2.08 (1H, m), 2.01 - 1.91 (1H, m). ^{13}C NMR (101 MHz, DMSO-d_6) δ 157.3, 140.9, 130.4, 129.2, 128.3, 126.6, 126.3, 125.3, 122.9, 122.6, 122.5, 115.6, 112.5, 79.0, 47.9, 38.1, 36.5. ^{19}F NMR (376 MHz, DMSO-d_6) δ-60.08.

Crystallization of TREK-2 in complex with fluoxetine derivatives

A 50 mM stock of Br-fluoxetine or norfluoxetine (Sigma-Aldrich) was dissolved in SEC buffer without detergent. This was added to the protein to give a final compound concentration of 5 mM and protein concentration of 9-11 mg/ml. Protein was incubated with compound for 3 h at 4 ºC prior to crystallization. Crystals were grown as for form 1 and 2 crystals with protein::reservoir ratios of 2:1 and 1:1 at 4°C. The norfluoxetine co-crystals grew from a reservoir solution containing 0.2 M ammonium formate, 0.1 M Tris, pH 7.0 and 30 % (w/v) pentaerythritol ethoxylate (15/4) at 4°C. Crystals were cryo-cooled directly from reservoir solution with added detergent (0.2 % OGNG / 0.02 % CHS). For the Br-fluoxetine derivative, reservoir solution contained 0.1 M MES buffer, pH 6.5, 0.05 M magnesium chloride, 1mM $CdCl_2$ and 14-30 % PEG500DME. Both plate ($P2_12_12_1$) and prism ($P2_1$) morphologies were observed in identical drops, however the plate morphology diffracted to higher resolution. Crystals were cryo-cooled by stepwise transfer into artificial mother liquor containing increasing concentrations of PEG500DME (0.2 M potassium chloride, 0.2 % OGNG/0.02% CHS, 0.1 M MES, pH

6.5, 1 mM $CdCl_2$, 14-30% PEG500DME). The PEG500DME concentration was increased in 5 % steps up to 30 %. 5 mM Br-fluoxetine was added to the cryo-solution in the final 30 % PEG500DME soak solution. Crystals were rapidly cryo-cooled in liquid nitrogen.

Structure determination and refinement for the form 1 crystals

All crystallographic data were collected at 100 K on either I02 (norfluoxetine complex) or the I24 microfocus beamline (Diamond Light Source) with a fine phi slicing strategy and processed with XDS (*34*) and AIMLESS (*35*). Form 1 crystals diffracted anisotropically with diffraction spots to 3.2 Å in the best direction and 4.1 Å in the worst direction (nominal resolution 3.4 Å; limits based on Mn (I/σI) >2 criteria - see Table S1). The crystals belong to space group $P2_1$ and contain two channel homodimers per asymmetric unit. Initial phases were obtained using molecular replacement with a search model ensemble comprising the transmembrane regions of TRAAK/K2P4.1 (3UM7) and TWIK-1/K2P.1 (3UKM) monomers in PHASER (*36*). Initial maps, calculated from the poly-alanine truncated PHASER solution, clearly revealed electron density for the extracellular cap domain region and allowed placement of both cap helices (EC1/EC2) for each chain. Subsequent rounds of refinement and model building, carried out with COOT (*37*), allowed connection of the cap helices and placement of the majority of sidechains. The chain trace was verified by treatment of crystals with 1 mM sodium ethylmercurithiosalicylic acid (EMTS) overnight which gave clear labeling at a single solvent-exposed cysteine (Cys^{249}) in M3 (see fig. S2D). Both prime-and-switch maps (PHENIX (*38*)) and interactive B-factor sharpening in (COOT (*37*)) were indispensable in the model building process. Two strong peaks that were present in both the 2mFo-DFc / mFo-DFc and anomalous difference electron density maps were assigned to cadmium ions that mediate lattice contacts between the cap domains of two adjacent homodimers in the crystal (fig S2D). The connection of the two cap helices and the intermolecular disulfide bridge between Cys^{123} of each monomer could also be clearly resolved and results in a domain-exchanged topology for the TREK-2 homodimer (fig. S5). Elongated tubes of persistent electron density, bound between M3 and M4, were modeled as the alkyl chains of a single phospholipid moiety. While there are indications of lipid density on both homodimers, alkyl chains have only been modeled for the AB homodimer.

Refinement was carried out with BUSTER (v. 2.11.2) (*39*) using all data to 3.2 Å with NCS restraints and a single TLS group per protein chain. The structure was refined to R/R_{free} values of 23.7 / 25.4 %, with good model geometry (Table S1). The final model comprises two channel homodimers per asymmetric unit, encompassing residues Lys^{73}-Lys^{333}, each containing four potassium ions within the selectivity filter. The putative glycosylated region around Ser^{150} in the extracellular cap domain is completely disordered in all molecules, the M2-M3 connecting region (residues 229-235) is not ordered in chains A and C, and the filter2-M4 connecting loop (residues 293-298) is only fully ordered in the AB homodimer. The model has excellent geometry as assessed by the MOLPROBITY server (*40*) with 97.5 % of residues located in favored regions of the Ramachandran plot and no outliers.

Determination of Cap connectivity for the form 1 crystals

The electron density maps calculated for the cap region of the Form 1 crystals is sufficiently well resolved to unambiguously trace the main chain and confirm the domain-exchanged arrangement previously observed for the TRAAK-Fab structure (Fig. S5). Clear interpretation is aided by the fact that in the form 1 crystals the cap domain is stabilized in the crystal lattice by a sizeable intermolecular contact between the C-terminal ends of the EC1 helices (from chains B and D on adjacent homodimers) that is mediated by two cadmium ions from the crystallization solution (Fig. S4A). The geometry of the connecting disulfide bridge falls within the standard left-handed spiral classification based on the chi2, chi3, chi2' angles (*41*).

Structure determination and refinement for the form 2 crystals

The coordinates of a channel homodimer from the 3.4 Å Form 1 crystal form were used as a molecular replacement search model in PHASER (*36*). Form 2 crystals also contain two channel homodimers in the asymmetric unit although one dimer is considerably less ordered and has much higher overall temperature factors (Table S1). Initial electron density maps indicated a large shift in the position of M4 in the Form 2 structure and so the search model was truncated at Gly312 and the sidechains were removed prior to calculation of a prime-and-switch map in PHENIX (*38*). The positions of M2, M3 and M4 were adjusted in the better resolved dimer and sidechain positions were built *de novo*. The resultant dimer was then used as a template to build the less ordered dimer. Refinement was carried out with BUSTER (v. 2.10.1) (*39*) using all data to 3.8 Å with NCS restraints and a single TLS group per protein chain. In addition, individual temperature factors were refined as this was found to improve R_{free}. Electron density within the selectivity filter was modeled by three potassium ions. No density was observed for the most extracellular K^+ ion position in the filter. B factor sharpening in COOT (*37*) was used to improve the quality of the electron density maps so that sidechains could be assigned. Elongated tubes of electron density were observed between M3 and M4 and penetrating into the intracellular pore vestibule across the pore axis. This density has been assigned to partial lipid alkyl chains. The final model has been refined to acceptable R/R_{free} values and geometry (Table S1). In addition to the density that has been assigned to the lipid chains Lip1, 2 and 3, there is additional density in the vestibule and on the outer surface of the channel in the 3.9 Å down state structure, which could represent detergent molecules or more bound lipids, but at this resolution interpretation of the density was not possible.

Norfluoxetine and Br-fluoxetine complex structure determination

The coordinates of a channel homodimer from the Form 2 crystal form were used as a molecular replacement search model in PHASER (*36*). The models were rebuilt in COOT (*37*) and refined with BUSTER (v. 2.10.1) (*39*) as described for Form 2. Using data collected from co-crystals of the Br-fluoxetine derivative at a wavelength close to the bromine K edge (λ=0.886Å) we unambiguously resolved the positions of the bromine atoms using anomalous difference electron density maps. Anomalous peaks were evident in all but one of the fenestrations (Fig S9A**)** indicating bound ligand (each channel homodimer contains two lateral fenestrations). Additional anomalous peaks were observed between the cap domains of adjacent dimers which correspond to the two

cadmium ions that mediate lattice contacts. Guided by the anomalous peaks, the tri-fluoro-methylated phenoxyl group of the Br-fluoxetine ligand was unambiguously modelled into all 4 fenestrations (the Br-fluoxetine crystals contain two channel homodimers in the asymmetric unit). The remainder of the ligand appears to be disordered with little or no electron density even in sharpened maps and has not been modelled. The bromine atoms were manually assigned an occupancy of 0.8 to account for signs of radiation damage.

The norfluoxetine complex was crystallized in the same spacegroup as the Form 2 down state. Initial electron density maps showed evidence of ligand binding in a similar position within the fenestration to that observed in the Br-fluoxetine derivative. The density was relatively weak in the initial BUSTER maps (Fig. S9H), but could clearly be resolved using both B-factor sharpening in COOT, and REFMAC and RESOLVE density-averaged maps (Fig. S9 E-G). Initially, norfluoxetine was modelled into the density in the best resolved site between M4 of chain A and M2 of chain B. As the norfluoxetine used for co-crystallization was a racemic mixture, both R- and S- forms were modelled with equal occupancy. Multiple binding modes were initially explored but a single orientation similar to that observed for the Br-fluoxetine gave the best fit based on both density-fit and refinement behavior. This binding mode was then used to account for the weaker electron density in the three other fenestration sites. Ligand coordinates and restraint files were generated using the GRADE web server (http://grade.globalphasing.org). Molecular graphics were generated using either PyMol (*42*) or the UCSF Chimera package (Fig 2CD) (*43*).

Molecular dynamics simulations

Models of the TREK-2 up and down states were created using the crystallographic structures with missing atoms and loops were added back in most favored position without clashes using COOT (*37*). The up state was modeled by taking chain A and chain B of 4BW5. The missing M2-M3 loop (226-231) of chain A was modeled based on chain B, with the cap-M2 connection, residues 149 to 152 modeled based on residual electron density present for chain C. The TREK-2 down state chain A cap-M2 loop (residues 150-154), M2-M3 loop (residues 226-230) whereas chain B cap-M2 loop (residues 149-154), TM2-TM3 loop (residues 226-231), and pre-M4 loop (residues 292-297) were modeled in MD simulations using Modeller 9v9 (*44*). The resulting models were converted to coarse-grained (CG) (Martini v2.1) representations and CG-MD simulations then performed for 500 ns at 323 K to permit the assembly and equilibration of a bilayer containing POPC (1-palmitoyl-2-oleoyl-sn-glycero-3-phosphocholine) lipids around the embedded membrane protein. The POPC head groups were altered to POPC:POPE (4:1) in the extracellular leaflet and POPC:POPE:POPS (3:1:1) in the intracellular leaflet and additional coarse grain simulation was conducted for a total of 1 μs. The protein and lipids were next converted to atomistic structures using the CG2AT method described previously (*45*). The initial system was solvated with SPC water and 150 mM KCl, and three K^+ ions at position S0, S2 and S4 in the selectivity filter, whereas two water molecules were also added to the filter at the S1 and S3 positions. Atomistic simulations employed the GROMOS 53A6 united-atom force-field with SPC water (*45, 46*). The atomistic system was equilibrated for 2 ns with the non-hydrogen atoms of the protein restrained at constant pressure (1 atm) and temperature (310 K) before the 100ns

unrestrained MD simulation with a timestep of 2 fs and a second 100ns simulation was repeated by randomizing initial velocity of the system. The interactions of lipids with the surface of the embedded membrane protein were evaluated with 100 ns MD simulations in which the protein conformation was restrained (via positional restraints to the C-α atoms (force constant 1000 KJ/mol/Å)). Normalized lipid densities were calculated for these simulations from the density of carbon atoms of the POP* lipids using the Volmap plugin tool with a 1 Å grid spacing.

Electrophysiology

Full length human TREK-2 (NP_612191) and the ORF encoding the truncated crystal construct were each cloned into the pBF oocyte expression vector which adds the 5' and 3' UTR sequences of the *Xenopus* β-globin gene. Mutagenesis was performed on full length TREK-2 and all mutations verified by automated sequencing. Capped mRNAs were then prepared by in vitro transcription using the AmpliCap SP6 High Yield Message Maker Kit (CamBio). Oocytes were prepared by collagenase digestion and manual defolliculation, and rinsed in ND96 solution prior to injection with the mRNA of interest; ND96 solution contained (in mM): 96 NaCl, 2 KCl, 1.8 $CaCl_2$, 1 $MgCl_2$, 10 HEPES (pH 7.4). Cells were typically injected with 0.1-2 ng of mRNA and currents were recorded 12-24 h following injection. Giant-patch electrodes were pulled from thick-walled borosilicate glass (Harvard Apparatus) and polished to give pipette resistances around 0.5-1 MΩ when filled with pipette solution. Pipette solution contained (in mM) 116 NaCl, 4 KCl, 1 $MgCl_2$, 1.8 $CaCl_2$, 10 HEPES (pH 7.4); whilst bath solution contained (in mM) 120 KCl, 1 NaCl, 2 EGTA, 10 HEPES (pH 7.3). For measurement of intracellular pH-sensitivity the bath solution was adjusted to the indicated pH. Patches were perfused with solution via a gravity flow perfusion system. Arachidonic acid (Sigma) was dissolved in DMSO and freshly diluted to the working concentration each day. Data were acquired with pClamp v10 (Molecular Devices), currents were recorded using an Axopatch 200B (Molecular Devices), filtered at 1 kHz and sampled at 10 kHz (Digidata 1322A, Molecular Devices). Macroscopic currents from inside out patches were recorded from 250 ms voltage steps to 0 mV from a holding potential of -80 mV unless otherwise indicated. Data are presented as the mean ± S.E.M.. Percentage inhibition was calculated from stable basal currents following excision using the following equation: % inhibition = $100(1-(I_{inhibited}/I_{basal}))$, where $I_{inhibited}$ refers to the recorded current in each concentration of norfluoxetine and I_{basal} refers to the measured current prior to drug administration. For tests of mechanosensitivity -11mmHg of negative pressure (calibrated using a Druic DPI260 Pressure Indicator) was applied through the patch pipette manually. Fold activation was calculated from the following equation: Fold activation = $I_{activated}/I_{basal}$, where $I_{activated}$ refers to the current level following application of activating stimuli and I_{basal} refers to the stable basal current. For measurement of whole cell currents using two electrode voltage clamp: electrodes were pulled from thick-walled borosilicate glass and filled with 3 M KCl. ND96 bath solution was used for all recordings; pH was adjusted using either NaOH or HCl. Oocytes were perfused with bath solution via a peristaltic pump perfusion system. Data were acquired with pClamp v10; currents were recorded using a GeneClamp 500 amplifier (Molecular Devices) and digitized using a Digidata 1322A. Current-voltage recordings were made by stepping membrane voltage from -120 mV to +60 mV in 10 mV increments for 300 ms

from a holding potential of -80 mV. For measurement of extracellular pH sensitivity the membrane potential was ramped from -150 mV to +50 mV from a holding potential of -100 mV. Experiments were performed at room temperature (18-22 °C). All traces were analyzed using Clampfit and are presented as mean ± SEM. All mutants tested for pHext response had similar levels of basal activity compared to WT TREK-2. Planar lipid bilayer experiments were performed using a Port-a-Patch automated planar patch clamp system (Nanion Technologies GmbH). The internal buffer was 200 mM KCl, and 10 mM HEPES pH 6.0, the outside buffers was 200 mM KCl, 10 mM HEPES pH 6.0. Giant unilamellar vesicles (GUVs) of DPhPC with 10% cholesterol were made by electroformation in an ITO coated glass chamber using the Vesicle Prep Pro (Nanion Technologies GmbH). Channels were incorporated by incubating the GUVs with purified TREK-2 for an hour after which detergents were removed by incubation with bio-beads SM-2 (Bio-Rad Laboratories). The Port-a-Patch was connected to an Axon Axopatch 200B amplifier; data were filtered at 5 kHz and recorded with a 100 kHz sampling rate.

Supplementary Text

Additional author notes

YYD and ACWP contributed equally to this project. YYD was responsible for purification optimization and preparation of protein, growth and optimization of crystals for the two unliganded conformations and for the norfluoxetine complex. ACWP supervised crystallization, mounted and screened crystals, collected diffraction data and solved and built the structures. AM was responsible for preparation of protein, growth and optimization of crystals for the Br-fluoxetine data and structure determination for this complex. CM was responsible for generation of all the electrophysiology data and AM and CM made the same level of contribution to this paper. PA performed and MSPS and SJT supervised the MD simulations. AQ was responsible for running the HTP IMP pipeline and, together with MG and LD, generated initial expression and purification optimization data. SG cloned the constructs used in this experiment. SM produced large scale insect cell cultures and the baculovirus necessary for structure determination. GFR and PEB designed the synthesis of Br-fluoxetine, GFR synthesized and PEB supervised the synthesis of Br-fluoxetine. MVC and LC performed functional assays on purified TREK-2 using the Port-a-patch. CB initiated the project, helped in project management and helped prepare the manuscript. NABB was responsible for managing the pilot stages of this project, including cloning and test expression; and production of insect cells cultures. SJT was responsible for managing the electrophysiology and other functional data. EPC was responsible for managing all aspects of the structural work. She designed constructs, collected X-ray data and contributed to structure solution. YYD, ACWP, SJT and EPC analyzed the data and prepared the manuscript.

Extended acknowledgements

We thank members of the SGC Biotech team, including Claire Strain-Damerell for mutagenesis and detergent screening and preparation of insect cell cultures. We thank Brian Marsden and David Damerell for bioinformatics support, Rod Chalk and Georgina Berridge for mass spectrometry and Aled Edwards for suggesting the use of 8-bromo-fluoxetine for binding site identification. We thank staff at Diamond Light Source Ltd. in particular the microfocus beamline staff Danny Axford, Robin Owen and Gwyndaf

Evans. PA is supported by a Wellcome Trust OXION Training Fellowship and MVC by a Carlsberg Foundation Fellowship. AM is supported by an EPSRC Life Sciences Interface Doctoral Training Centre studentship (EP/I017909/1).

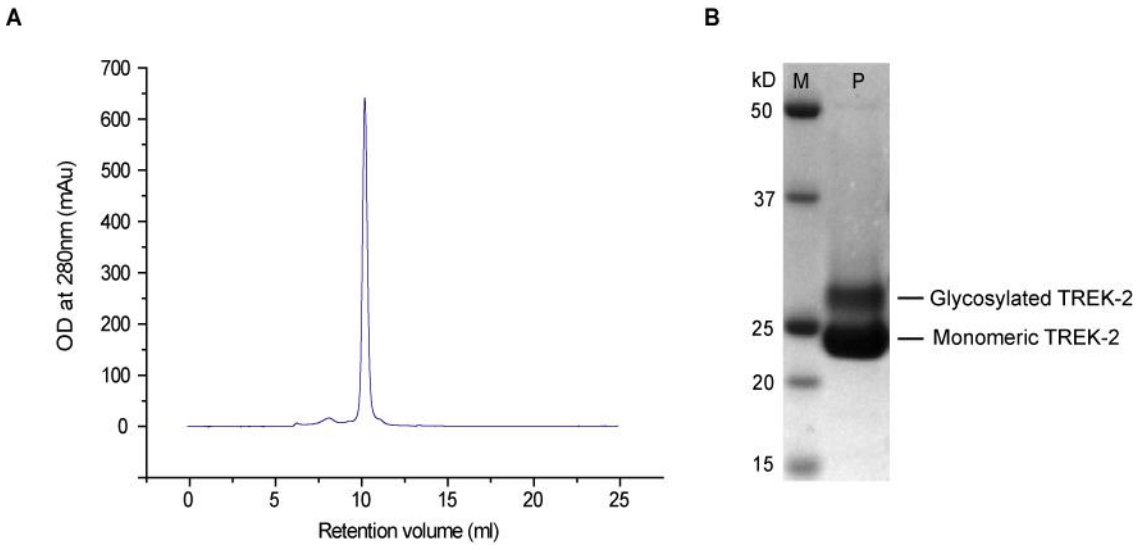

Fig. S1

Purification of TREK-2. **(A)** Size exclusion chromatography (SEC) profile for TREK-2 and (**B**) SDS-PAGE analysis of final pooled material (P) showing that the protein used in crystallization is partially deglycosylated by PNGaseF. M indicates protein molecular weight markers.

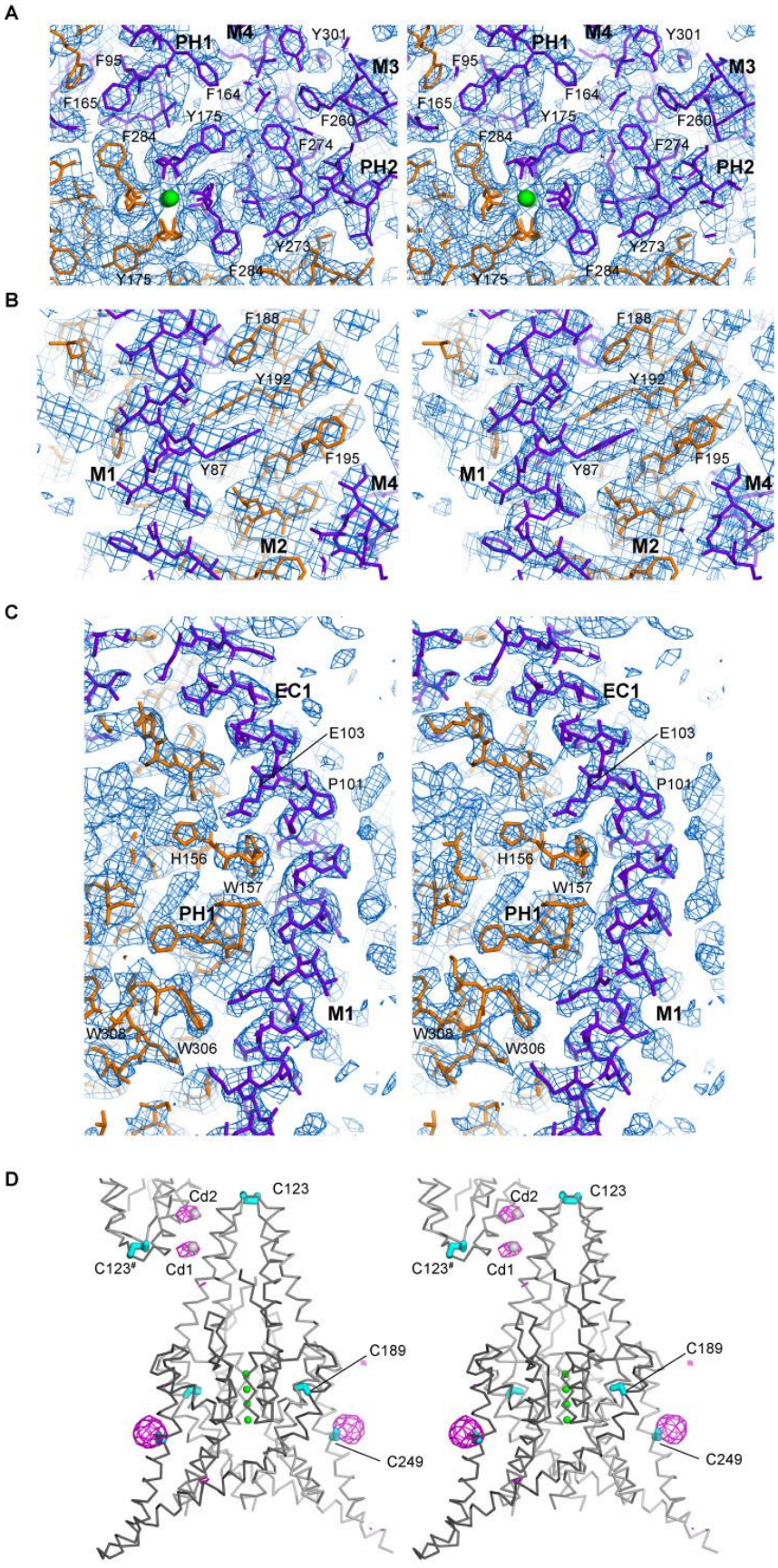
A
PH1
M4
Y301
F95
M3
F165
F164
Y175
F260
F284
F274
PH2
Y273
Y175
F284
B
F188
Y192
M1
Y87
F195
M4
M2
C
EC1
E103
P101
H156
W157
PH1
M1
W308
W306
D
Cd2
C123
C123#
Cd1
C189
C249

Fig. S2

Quality of electron density for the up state 3.4 Å TREK-2 crystal structure. (**A-C**) Representative views of electron density around the pore (**A**), M1-M2 interface (**B**) and M1-EC1 helices (**C**). The electron density map shown is a simulated-annealing, composite omit map calculated in PHENIX, contoured at 1.2σ (**A, B**; for clarity) or 1σ (**C**) and overlaid on the final model. (**D**) 6 Å anomalous difference map calculated from data collected from a crystal soaked with 1 mM EMTS. The electron density (magenta) is contoured at 3.5 σ. The solvent-exposed Cys^{249} located in M3 of each monomer is clearly identified by strong anomalous peaks (>10σ). The other two cysteines (cyan) present in TREK-2 are not labelled under these conditions – Cys^{123} forms an intermolecular disulphide bridge with its counterpart in the homodimer and Cys^{189} (M2) is completely buried. Two cadmium ions (Cd1/Cd2) from the crystallization solution, mediating lattice contacts between the cap domain EC1 helices of adjacent homodimers, are also identified in the anomalous difference map by weaker (ca. 5σ) peaks.

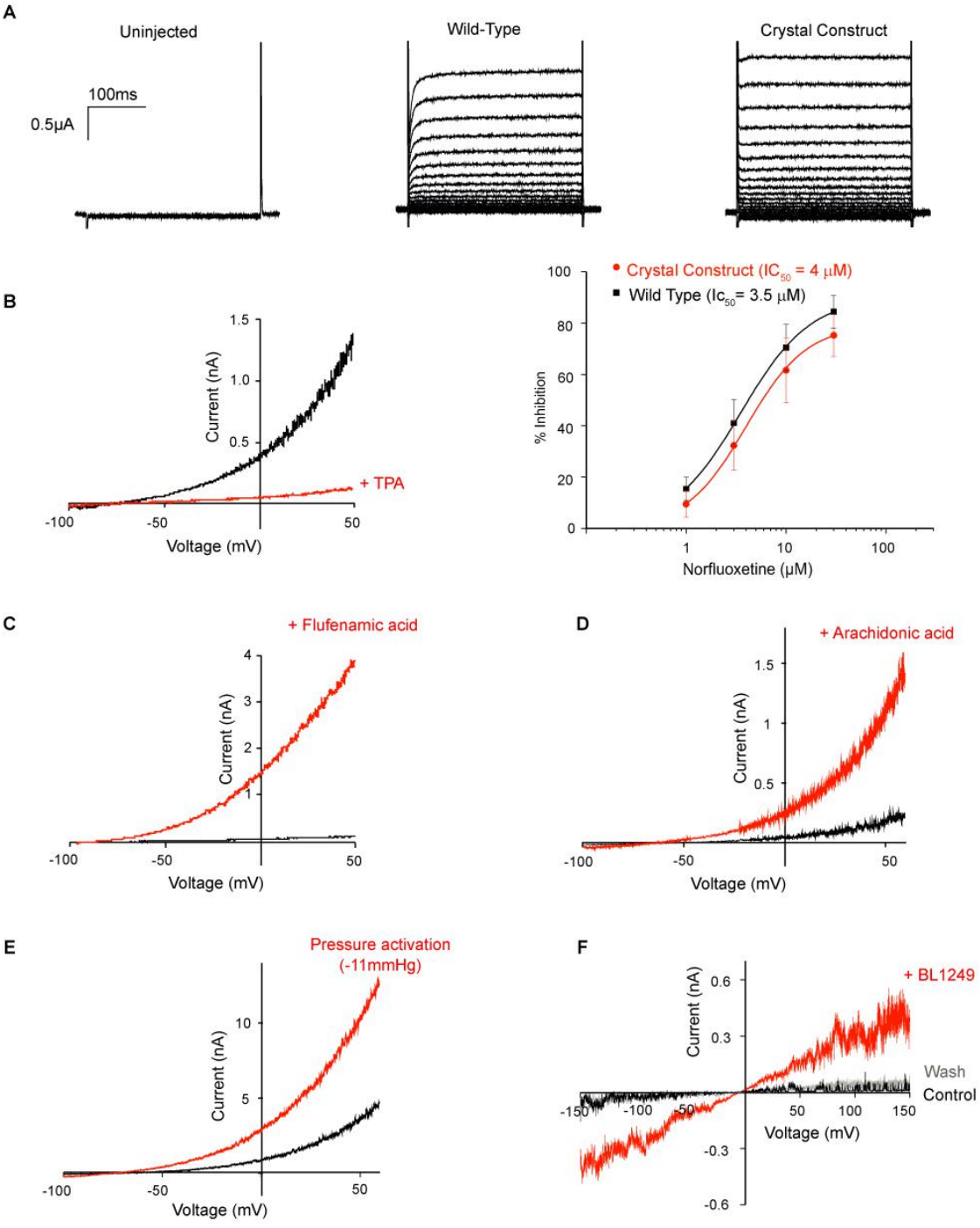
A
Uninjected
Wild-Type
Crystal Construct
100ms
0.5µA
B
Current (nA)
+ TPA
Voltage (mV)
Crystal Construct (IC50 = 4 µM)
Wild Type (Ic50= 3.5 µM)
% Inhibition
Norfluoxetine (µM)
C
+ Flufenamic acid
Current (nA)
Voltage (mV)
D
+ Arachidonic acid
Current (nA)
Voltage (mV)
E
Pressure activation
(-11mmHg)
Current (nA)
Voltage (mV)
F
+ BL1249
Wash
Control
Current (nA)
Voltage (mV)

Fig. S3

Wild type and crystal construct length TREK-2 show similar behavior with a range of stimuli. (**A**) Current-voltage relationship from two electrode voltage clamp recordings of the WT and truncated crystal construct channels expressed in *Xenopus* oocytes. The membrane voltage was stepped from -120 mV to +60 mV in 10 mV increments for 300 ms from a holding potential of -80 mV. (**B**) A representative trace showing block of the crystal construct channel by 1 mM Tetrapentylammonium (TPA). The channels also retain inhibition by norfluoxetine. (**C**) Flufenamic acid (FFA, 1 mM) (*47*) and (**D**) Arachidonic acid (10 μM) both activate the crystal construct channels in inside-out patches. (**E**) Importantly, the truncated crystal construct also retains sensitivity to membrane stretch (-11 mm Hg). (**F**) Functional activity is also observed when the purified crystal construct protein is reconstituted into a lipid bilayer. The relative orientation of channels within the bilayer is not known but K^+ selective currents (black trace) can be activated by 1 μM BL1249, a TREK channel activator (*47*) (red trace). This effect is reversible (wash, grey trace). Currents were recorded using a 10 s ramp from -150 mV to +150 mV.

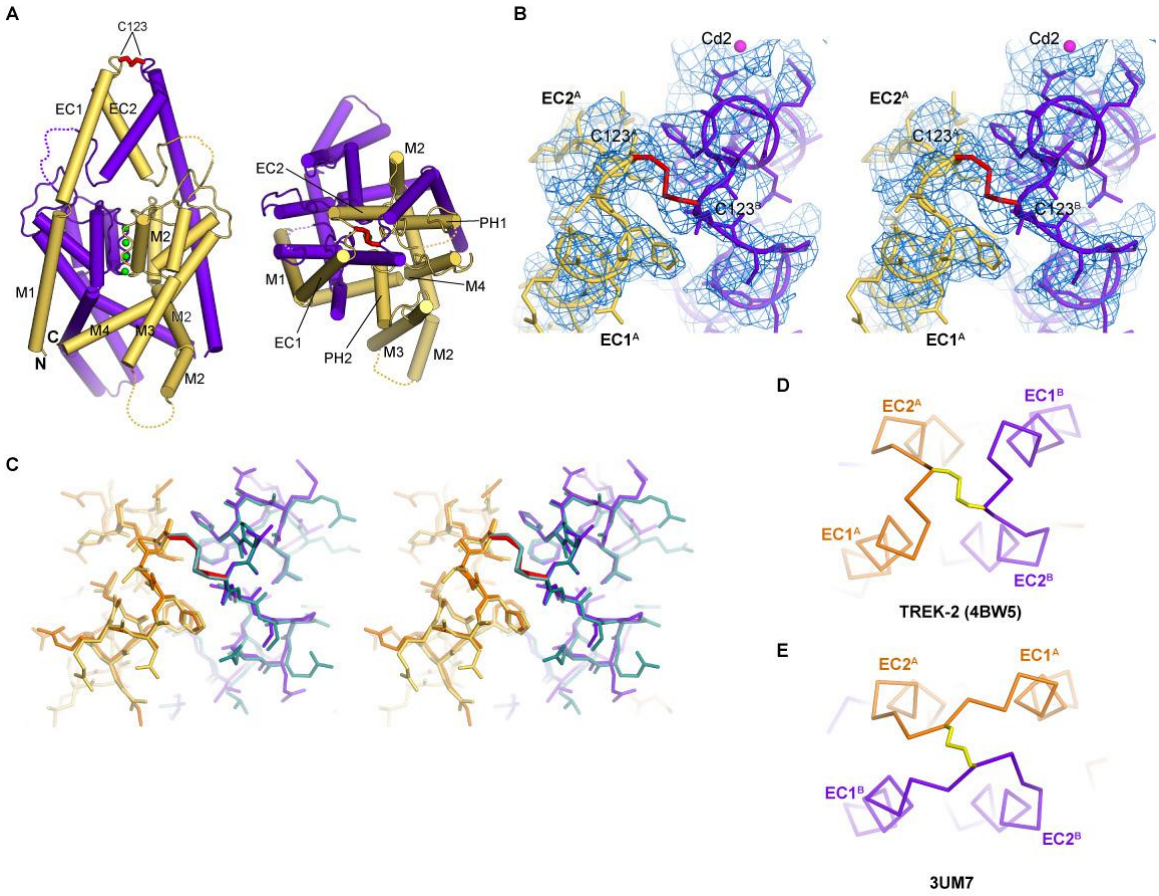

Fig. S4

The structure on TREK-2 in the vicinity of the disulfide bond at the distal end of the cap, is shown with electron density omit maps. The maps reveal a M1/EC1/EC2 domain-exchanged conformation similar to that seen in the 2.75Å TRAAK structure in complex with an antibody (pdb: 4I9W). (**A)** Schematic representation of 3.4 Å up state TREK-2 homodimer viewed in plane of membrane (*left*) and onto the cap from the extracellular side (*right*). (**B**) Stereo view of the electron density around the cap disulfide bridge. The 'omit' electron density map shown is calculated using the prime-and-switch method implemented in PHENIX (*38*) starting with a TREK-2 model that lacks the cap residues 118-127. The disulfide bridge between adjacent Cys^{123} residues is highlighted in red. Two cadmium ions (Cd1/2) stabilize the cap domain via lattice contacts between EC1 helices of adjacent homodimers (**C**) Superposition of the domain-exchanged cap domains of TREK-2 (yellow/purple) and 2.75 Å TRAAK structure (4I9W, orange/dark cyan). (**D**) Schematic view of cap connectivity for domain-exchanged TREK-2 (orange/purple) and (**E**) non-exchanged TRAAK (pdb: 3UM7).

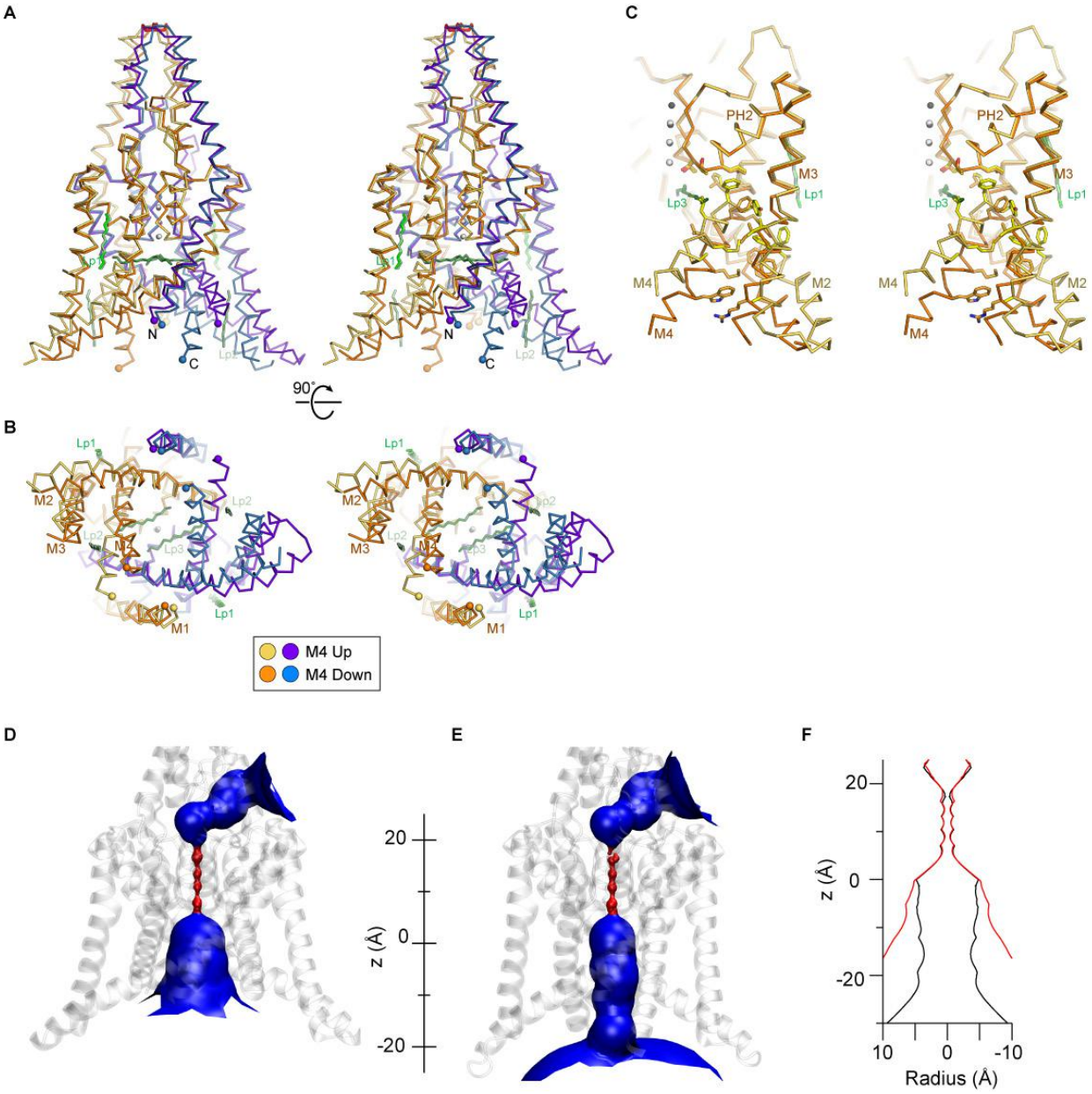
A
C
PH2
M3
Lp1
Lp3
M4
M2
N
C
Lp2
90°
B
M1
M4 Up
M4 Down
D
E
20
0
-20
z (Å)
F
10
Radius (Å)

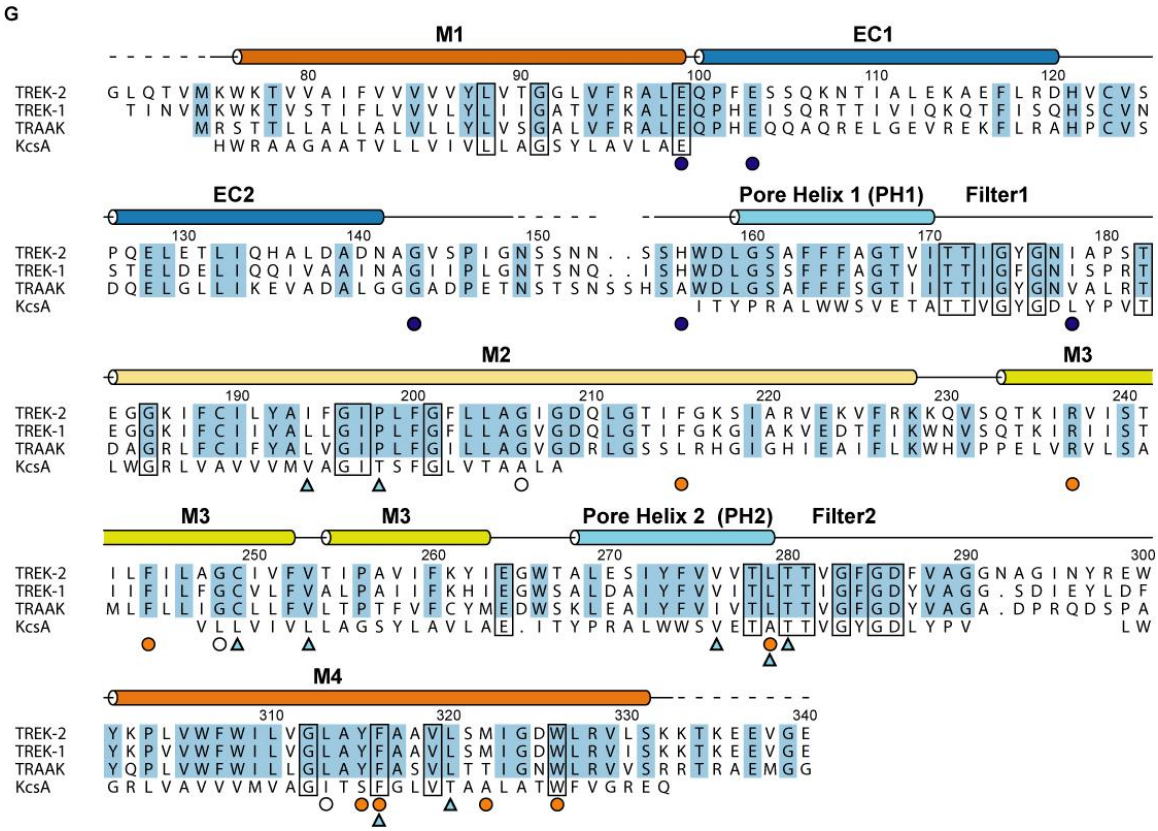

Fig. S5

Comparison of up/down conformational states of TREK-2 and an alignment of the TREK, TRAAK and KcsA sequences. **(A)** Stereo view of TREK-2 channel homodimers viewed from the plane of the membrane. Modelled alkyl chains representing lipid fragments (Lp1-Lp3) are colored green. Fragment Lp1 is observed in both crystal forms whereas Lp2/3 are restricted to the 'down' conformation. **(B)** Stereo view looking from the intracellular face towards the pore. **(C)** Stereo view of superposed TREK-2 monomers for 'up' (yellow) and 'down' (orange) states. Hole (*48*) profiles displaying the radius of the pore in the up **(D)** and down state (**E**) of TREK-2. Blue represents regions of the ion path with a radius of >3.5 Å and red <1.2 Å. (**F**) Plot of the radius of the inner pore in the up (red) and down (black) states. **(G)** Sequence alignment of human tandem two pore K channels TREK-2, TREK-1 and TRAAK, and the archetypal 2-TM KcsA. Only the M1/ Pore helix / filter / M2 regions of KcsA are shown based on structural superposition with TREK-2 model. Residues involved in the M2/3/4 hydrophobic clusters (orange circles), helix hinging residues (open circles), external pH sensor region (blue circles) and norfluoxetine binding site (cyan triangles) are highlighted.

A M4 UP, $P2_1$

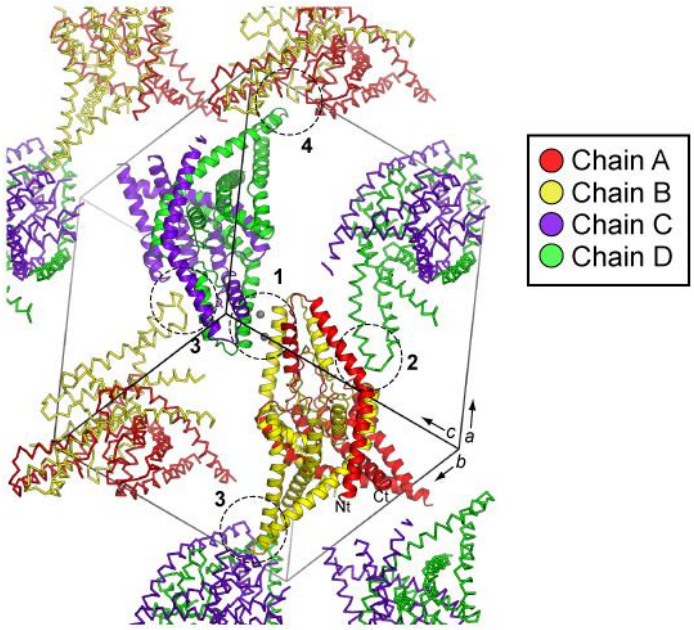

1 - Cap EC1 helix [B/D] mediated by Cd^{2+} ions
2 - Cap EC1 [A] with Cterm M2 [D]
3 - M2/M3 loop [B] with C-term M3 / Pore loop2 [C]
4 - SF1-M2 loop [B] with M2/3 loop [D]

B M4 DOWN (Apo / NFX), $P2_1$

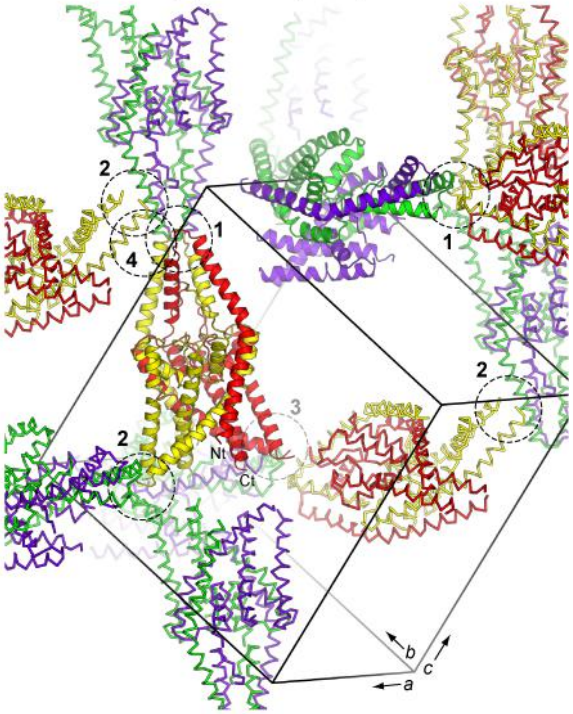

1 - Cap S-S tip [B/D]
2 - Cterm M2 [B] with EC1 [D]
3 - Cap tip [C] with Cterm M2 [A]
4 - Cterm EC1 [B] Cterm M2 [B]

C M4 DOWN, Br-FX, $P2_12_12_1$

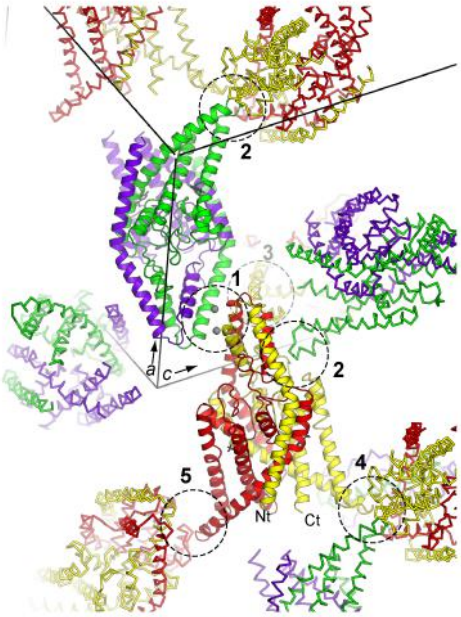

1 - Cap EC1 helix [A/D] mediated by Cd^{2+} ions
2 - M2 Cterm [D] with Cap/TMD loop / Cterm M3 / Pore loop2 [B]
3 - Nterm EC2 [A] with Cterm M2 [B]
4 - Cap/TMD loop [B] with M2/M3 loop [B]
5 - Cterm M2 [A] with Cterm M3 / PH2 loop [A]

Fig. S6

Protein-protein interactions between TREK-2 molecules in the three crystal forms. Schematic representations of the crystal packing contacts in the **(A)** Monoclinic Form 1 / 'up' state crystals, **(B)** Monoclinic Form 2 / 'down' state and norfluoxetine (NFX) co-crystals and **(C)** Orthorhombic 'down' state with brominated fluoxetine (Br-FX). All crystallographic asymmetric units contain two TREK-2 channel homodimers (shown in cartoon representation (AB dimer colored red/yellow; CD dimer purple/green)). Symmetry-related molecules are shown as thin ribbons. Crystal contacts, as defined by PDBePISA (*49*), are circled and numbered based on average interface area. Typically, the same regions of the channel, namely the cap domain helices and intracellular regions of the M2 and M3 helices, are involved in packing interactions within the crystal regardless of the conformational state. Helix M4 which exhibits the most dramatic reorientation in the 'up' and 'down' states is not involved in any crystal packing interactions. The most extensive protein-protein lattice interaction in the 'up' state monoclinic crystals **(A)** and 'down' state orthorhombic crystals is between the cap domains of adjacent dimers and is mediated by two cadmium ions (indicated by gray spheres) derived from the crystallization solution.

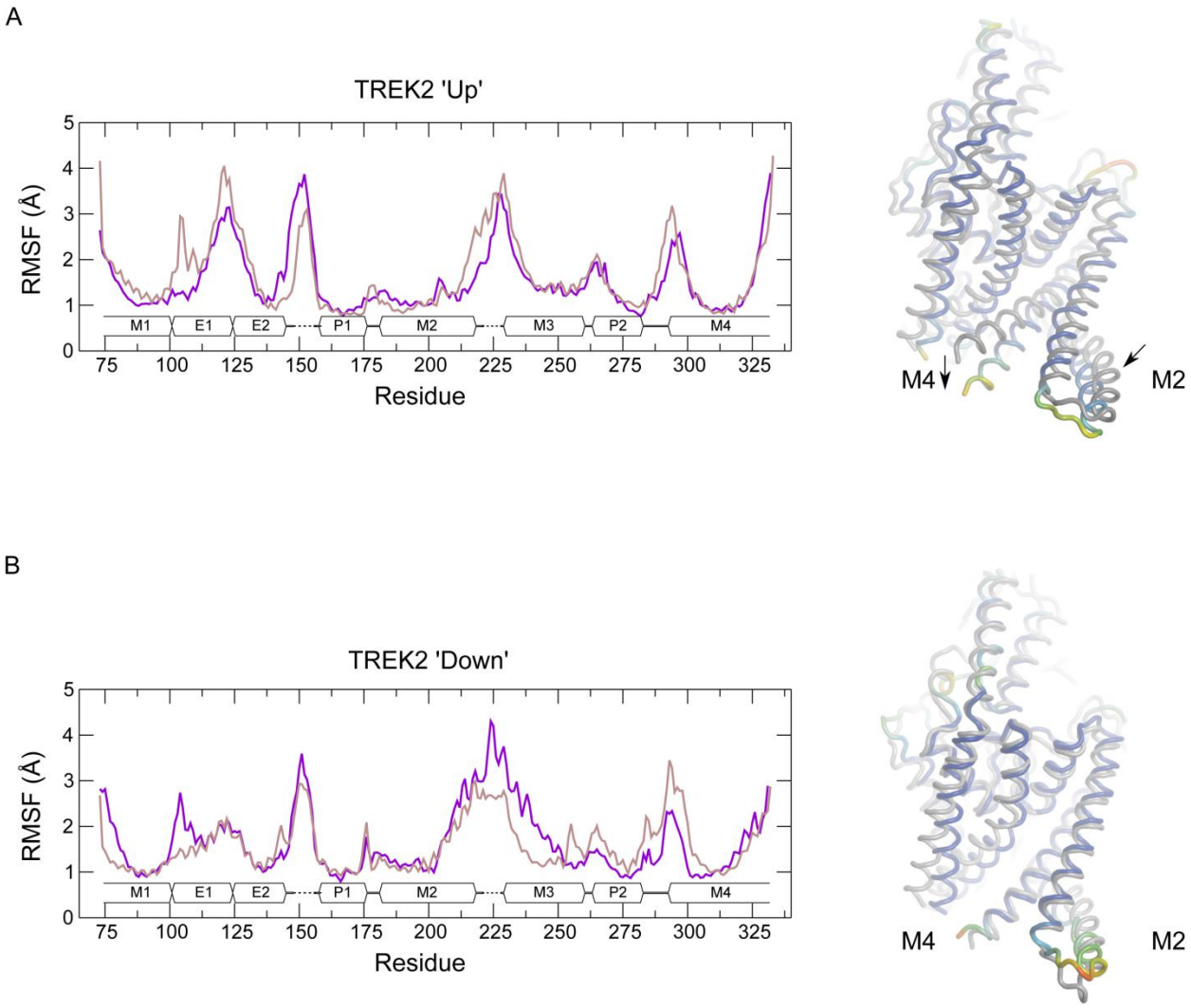

Fig. S7

Relative stability of 100ns MD simulation for TREK-2 up (**A**) and TREK-2 down (**B**) state structures in a lipid bilayer. Left panel: Averaged root mean square fluctuations (RMSF) calculated for backbone atoms of Chain A (purple) and Chain B (brown) from two 100 ns MD simulations versus residue number. The secondary structure of TREK-2 is also shown. Dashed lines represent regions missing in the crystal structures. Right panel: Tube representation of average structure from MD simulations colored by RMSF per residue (blue (small RMSF) through green to red (large RMSF)) superimposed on the starting structure (grey tube). Arrows indicate the movement of M4 and M2 in the up, but not down state simulations.

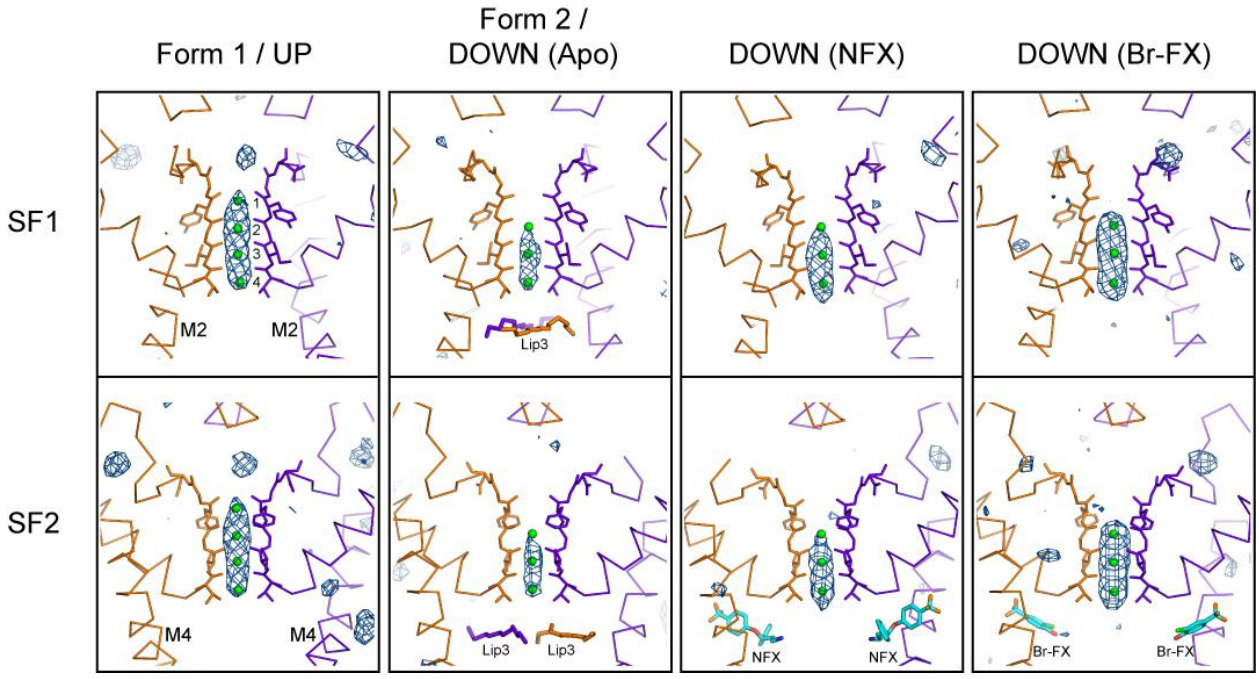

Fig. S8

Potassium ion occupation within the pore / selectivity filter for the various crystal forms. Omit electron density for the potassium ions (contoured at 3σ) is shown for the AB dimer in the Form 1, up state, where there are four potassium ions in the filter. Form 2, down state, norfluoxetine (NFX) and brominated fluoxetine (Br-FX) crystal structures, all of which have density for three potassium ions in the filter. Modelled potassium ions are shown as green spheres. Two views are displayed with either the selectivity filter 1 (SF1) (pore domain 1, residues 158-177) or SF2 (pore domain 2, residues 267-286) in the plane of the page. The lipid-like fragments (Lip3) observed in the Form2 down (apo) state form a barrier across the ion conductance pathway. In contrast, the norfluoxetine (NFX) and partially-ordered, brominated fluoxetine do not sterically block the pore axis.

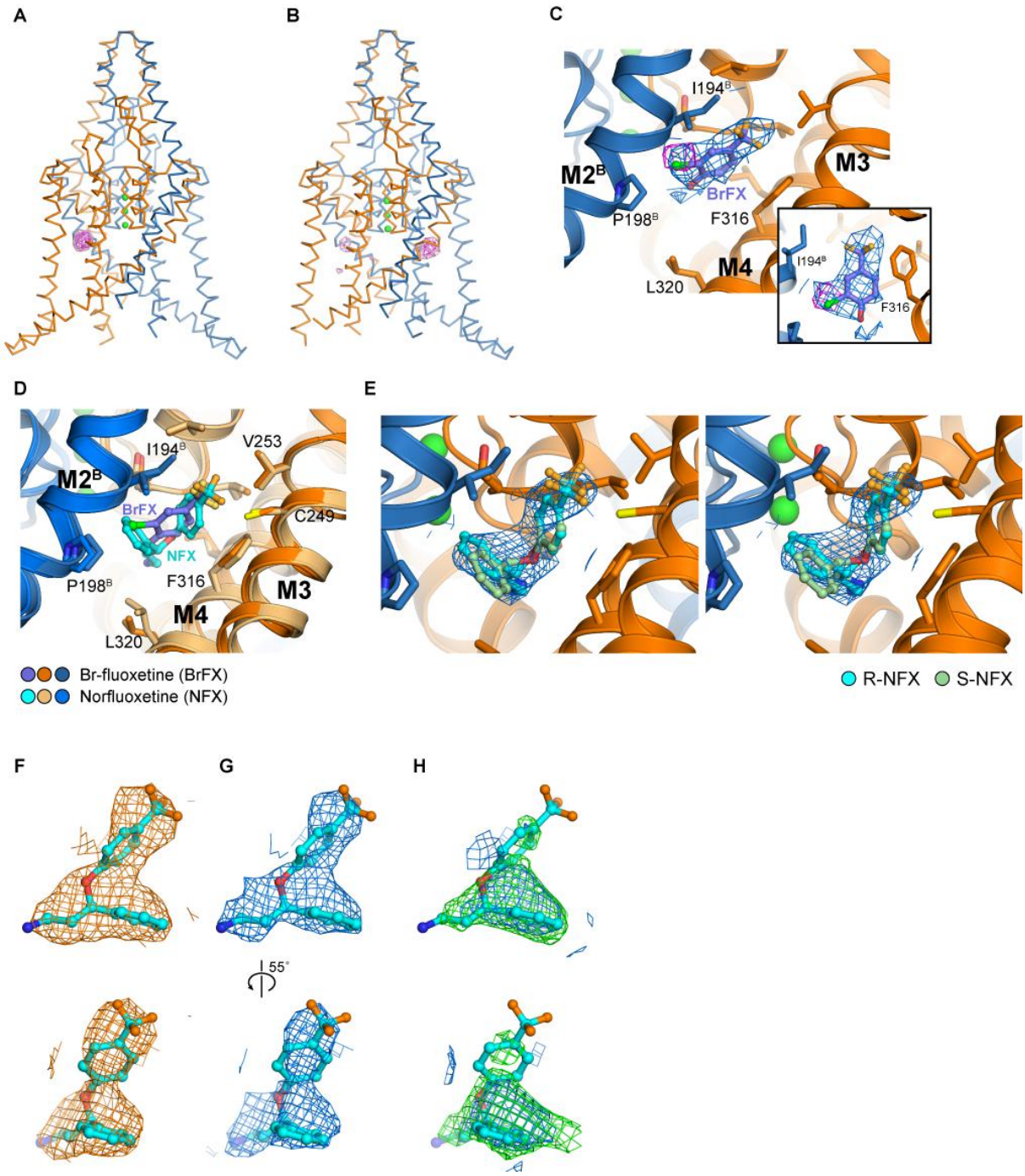
A
B
C
I194B
M2B
M3
BrFX
P198B
F316
M4
L320
I194B
F316
D
E
I194B
V253
M2B
BrFX
C249
NFX
P198B
F316
M3
M4
L320
Br-fluoxetine (BrFX)
Norfluoxetine (NFX)
R-NFX
S-NFX
F
G
H
55°

Fig. S9

Binding site for norfluoxetine unambiguously identified using anomalous signal from brominated derivative of fluoxetine. **(A-B)**. Anomalous difference map calculated at 5Å for the Br-fluoxetine (Br-FX) dataset (collected at the Br K-edge) and shown with the C-α trace for each TREK-2 dimer within the asymmetric unit (chain A/C – orange; chain B/D – blue). The 5 Å anomalous difference map is contoured at 4.5σ (magenta) and 3σ (pink). A single anomalous peak, corresponding to the location of the bromine atom of Br-fluoxetine, is seen in the AB dimer while the CD dimer has two peaks. **(C**) Omit electron density for Br-fluoxetine. The RESOLVE density modified electron density (1σ, blue), calculated prior to ligand modelling, is shown with the 5 Å anomalous difference density (6.5σ, magenta). The brominated tri-fluoromethyl phenyl ring is well-defined in the electron density whereas the other two substituents are poorly resolved. **(D)** Comparison of the binding modes of Br-FX (lilac carbons) and norfluoxetine (NFX, cyan carbons). The binding site is viewed looking into the side fenestration between M4 and M2. Only the R-enantiomer of NFX is shown for clarity. **(E)** Stereo view showing the quality of the initial 3.6Å NFX electron density. The RESOLVE density modified electron density (blue; contoured at 1σ), calculated prior to ligand modelling, is shown for NFX along with the final model. As NFX used for crystallization is a racemic mixture, both R- and S-enantiomers were modelled. **(F-H)** Omit 3.6Å sigma-A weighted 2FoFc and FoFc electron density for the best defined NFX molecule (in the AB dimer). The electron density maps were calculated prior to inclusion of NFX in the refined model using RESOLVE **(F)**, REFMAC5 with map sharpening **(G)** and BUSTER **(H)**. Electron density maps are contoured at either 1σ (2FoFc) or 2σ (BUSTER FoFc map in (H); green).

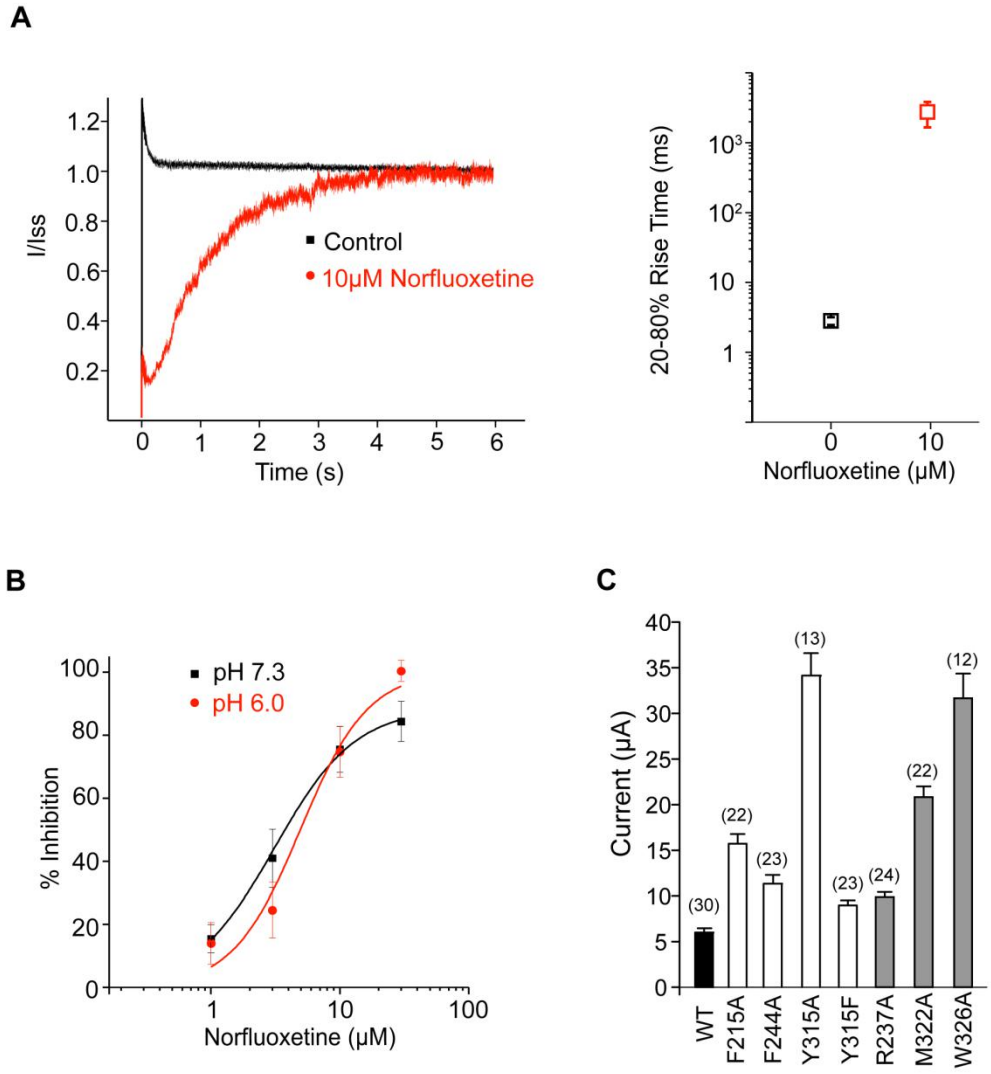

Fig. S10

Effect of norfluoxetine on the kinetics of TREK-2 activation by membrane stretch (-11 mmHg). (**A**) Left: In the absence of norfluoxetine rapid activation to a steady-state current (Iss) occurs within a few milliseconds. However, in the presence of 10 μM norfluoxetine the activation of inhibitor-bound channels to a steady state current is dramatically slower. The time taken for activation from 20 % to 80 % of the maximum steady state current is shown on the right and is 3 orders of magnitude slower in the presence of norfluoxetine. (**B**) By marked contrast to both stretch and AA activation (see Fig 2G), activation by pH_{int} (pH 6.0) does not alter norfluoxetine inhibition (see methods for details). (**C**) Basal whole-cell currents for the mutants described in Fig. 3F. Wild-type TREK-2 is shown for comparison. Currents were recorded at +100mV 24hrs after injection with 4ng of either WT or mutant mRNA.

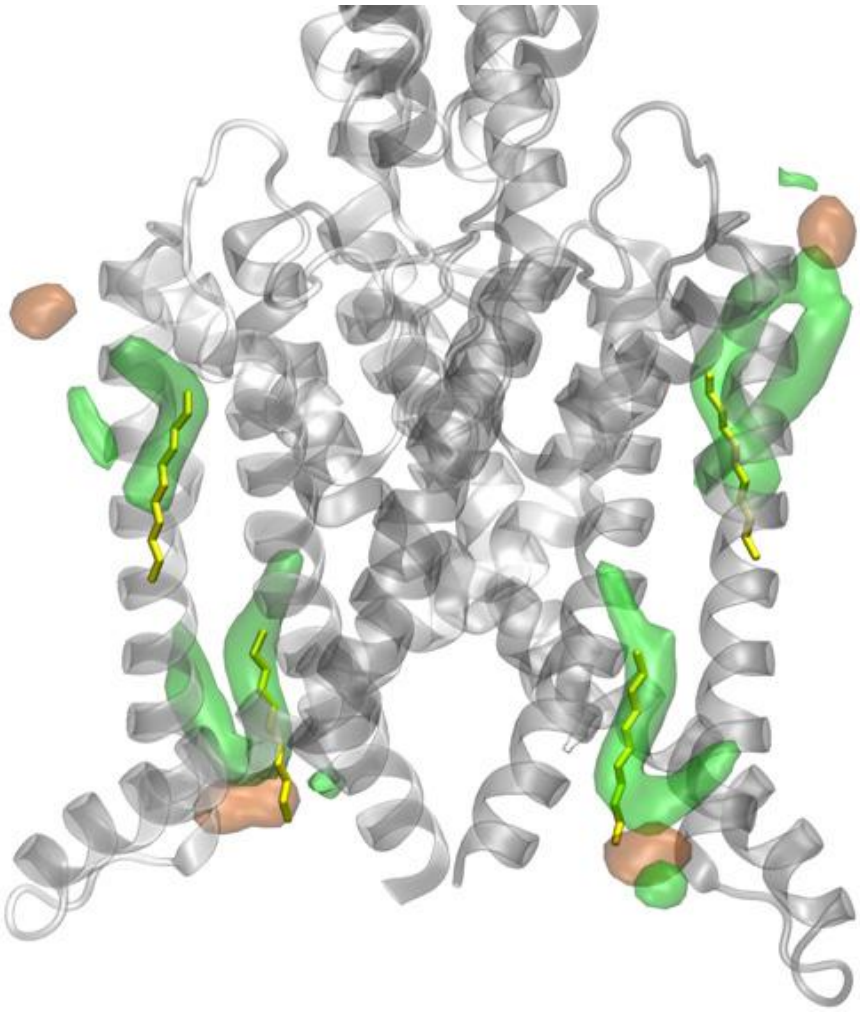

Fig. S11

MD simulations of lipid interactions. Lipid interaction during a 100 ns simulation with the protein positionally restrained. Transparent surface represents averaged density contour at 0.5 isosurface for carbon (green) and phosphorus (orange) atoms of lipids that interact at the sites overlaid onto the TREK-2 down state crystal structure. The modelled alkyl chains in the crystal structure are shown in stick representation (yellow). The high degree of overlap indicates that the alkyl chains modelled on the basis of elongated tubes of electron density probably represent immobilized lipids.

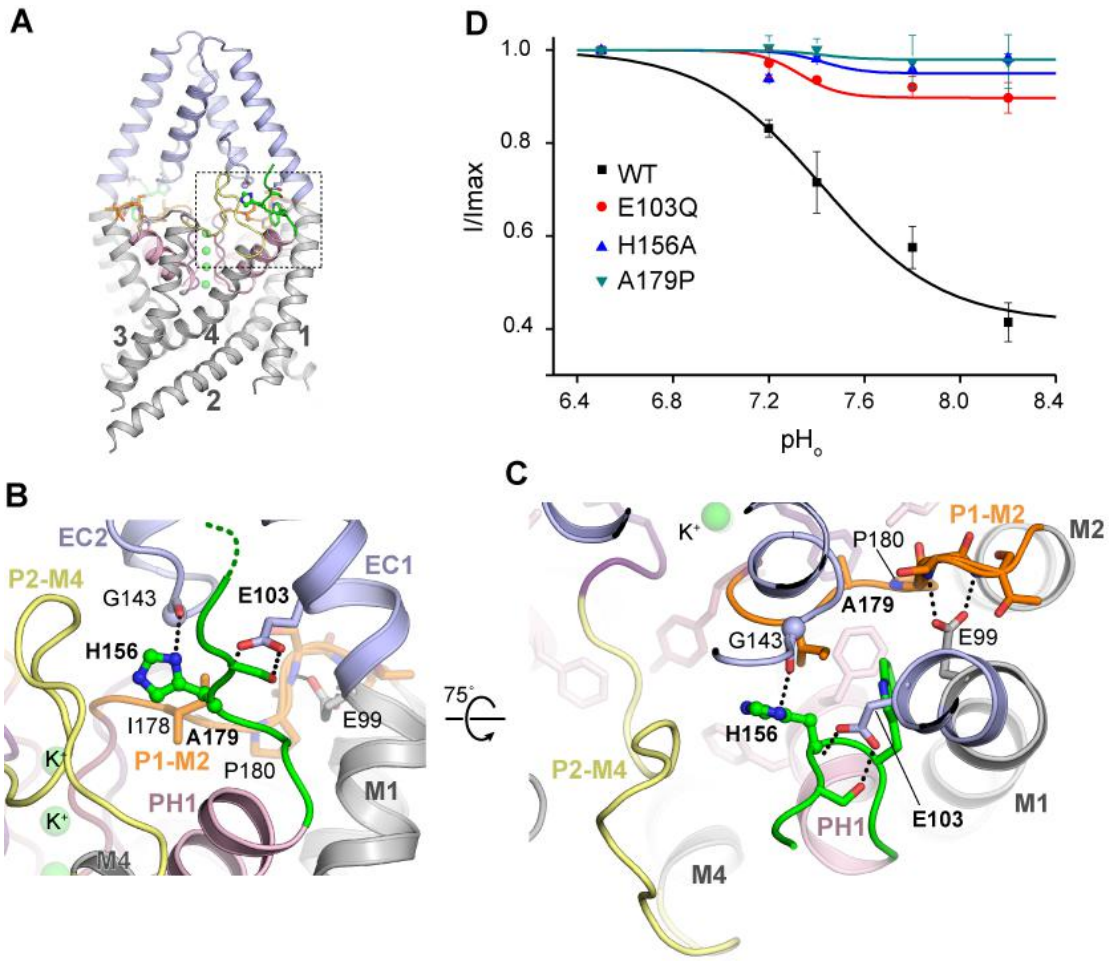

Fig. S12

The external pH sensor region centered on His^{156}. (**A**) The sensor histidine (His^{156}, green) is located between the ECD (pale blue) and pore helix 1 (PH1) of the transmembrane domain adjacent to the pore region (**B-C**). The environment round His^{156} is shown with different structural elements colored. Dotted lines represent hydrogen bonds. The filter loops P1-M2 and P2-M4 are colored orange and yellow respectively. (**D**) Effect of mutating residues within the His^{156} network or adjacent loops on external pH-sensitivity. These mutants have similar levels of basal channel activity, but markedly reduced pH_{ext} sensitivity. Consistent with the reported role for protonation of His^{156} in channel activation (*25*), the basal activity (recorded at pH_{ext} 7.4) of the H156A mutant was decreased by 22 ± 15 % compared to wild-type TREK-2. Basal whole-cell currents for the novel mutants described here (E103Q and A179P) were 10.5 ± 1.45 µA, and 7.6 ± 0.4 µA respectively, compared to 6.0 ± 0.5 µA for wild-type TREK-2.

Fig. S13

Synthesis scheme of Br-Fluoxetine (see methods for details of the synthesis).

Table S1

Data collection, phasing and refinement statistics.

	Form 1/up state	Form 2/down state	Br-fluoxetine complex	Norfluoxetine complex
PDB Code	4BW5	4XDJ	4XDL	4XDK
Data Collection				
Space group	$P2_1$	$P2_1$	$P2_12_12_1$	$P2_1$
Unit cell dimensions				
a, *b*, *c* (Å)	87.83, 96.96, 103.7	76.75, 113.90, 111.80	101.71, 109.84, 166.74	75.19,113.03,112.50
α, β, γ (°)	90, 92.58, 90	90, 90.97, 90	90, 90, 90	90, 90.41, 90
Resolution [Å][1]	3.2 (3.20-3.28)[1]	3.8 (3.80-3.90)[1]	3.5 (3.50-3.59)[1]	3.6 (3.60-3.69)[1]
Resolution limits [Å][2]	4.10, 3.33, 3.20	4.05, 3.80, 3.97	3.55, 3.5 ,3.91	4.33, 3.6, 3.6
	(3.82, 3.20, 3.20)	(4.00, 3.80, 3.88)	(3.50,3.50,3.82)	(4.09, 3.6,3.6)
Nominal Resolution [Å][3]	3.4	3.9	3.64	3.7
Total reflections	109355	63457	275680	82827
Unique reflections	28707	18910	24216	21872
Redundancy	3.8 (3.7)[1]	3.4 (3.4)[1]	11.4 (11.2)[1]	3.8 (4.0)[1]
Completeness [%]	99.4 (99.0)[1]	99.0 (99.5)[1]	99.9 (100)[1]	99.6 (99.6)[1]
R_{meas}[4]	0.062 (1.539)[1]	0.083 (0.971)[1]	0.097 (1.934)[1]	0.052 (0.931)[1]
$CC_{1/2}$	0.999 (0.436)	0.999 (0.579)	0.999 (0.553)	0.99 (0.685)
$I / \sigma I$	10.7 (1.1)[1]	10.8 (1.8)[1]	17.5 (1.5)[1]	15.1 (1.8)[1]
Refinement				
Resolution (Å)	39.57 – 3.20	37.26 – 3.8	35-3.50	40.0-3.60
No. reflections (free)	28689 (1458)	18895 (978)	24155 (1217)	21816 (1127)
R_{work} / R_{free}	23.69 / 25.40	26.29 / 27.69	23.52 / 26.33	24.76 / 25.41
No. atoms				
Protein	7203	6959	7474	6921
Other	32	99	92	214
B-factors (Å^2)				
Protein	156	167	157	182
Other	133	127	169	211
Dimer AB	148	139	150	159
Dimer CD	163	194	165	206
R.m.s. deviations				
Bond lengths (Å)	0.009	0.009	0.009	0.009
Bond angles (°)	0.93	0.90	0.93	0.91

[1] Values in parentheses are statistics for highest resolution shell

[2] Anisotropic resolution limits along each of the three principal directions as defined by AIMLESS based on Mn (I/sd(I)) > 2. Values in parentheses are resolution limits in each direction based on half dataset correlation > 0.5 ($CC_{1/2}$).

[3] Nominal resolution is defined based on overall Mn (I/sd(I)) > 2 as estimated by AIMLESS.

[4] R_{meas} is the redundancy-independent merging R factor

Movie S1

TREK-2 exhibits two distinct conformational states differing in the orientation of the transmembrane helices (M2-M4). The movie shows a linear transition between the up and down states of TREK-2, highlighting the structural differences between the two states and the concerted movement of the M2, M3 and M4 helices. A molecular surface representation illustrates the appearance of the lateral fenestrations observed in the down state structure. Norfluoxetine is shown in cpk representation binding in the fenestrations of the down state structure (cyan carbons). The models used for the movie have had missing loops that were not visible in the crystal structures reconstructed using structural information from other molecules in the asymmetric unit or from different crystal forms. The movie was created from a Cartesian morph between the up and down states calculated by UCSF-Chimera (*43*) and rendered using PyMol (*42*)**.**

References and Notes

1. P. Enyedi, G. Czirják, Molecular background of leak K^+ currents: Two-pore domain potassium channels. *Physiol. Rev.* **90**, 559–605 (2010). Medline doi:10.1152/physrev.00029.2009

2. A. Cohen, Y. Ben-Abu, N. Zilberberg, Gating the pore of potassium leak channels. *Eur. Biophys. J.* **39**, 61–73 (2009). Medline doi:10.1007/s00249-009-0457-6

3. J. Noël, G. Sandoz, F. Lesage, Molecular regulations governing TREK and TRAAK channel functions. *Channels* **5**, 402–409 (2011). Medline doi:10.4161/chan.5.5.16469

4. L. E. Kennard, J. R. Chumbley, K. M. Ranatunga, S. J. Armstrong, E. L. Veale, A. Mathie, Inhibition of the human two-pore domain potassium channel, TREK-1, by fluoxetine and its metabolite norfluoxetine. *Br. J. Pharmacol.* **144**, 821–829 (2005). Medline doi:10.1038/sj.bjp.0706068

5. C. Heurteaux, G. Lucas, N. Guy, M. El Yacoubi, S. Thümmler, X. D. Peng, F. Noble, N. Blondeau, C. Widmann, M. Borsotto, G. Gobbi, J. M. Vaugeois, G. Debonnel, M. Lazdunski, Deletion of the background potassium channel TREK-1 results in a depression-resistant phenotype. *Nat. Neurosci.* **9**, 1134–1141 (2006). Medline doi:10.1038/nn1749

6. Z. Es-Salah-Lamoureux, D. F. Steele, D. Fedida, Research into the therapeutic roles of two-pore-domain potassium channels. *Trends Pharmacol. Sci.* **31**, 587–595 (2010). Medline doi:10.1016/j.tips.2010.09.001

7. M. E. Henry, M. E. Schmidt, J. Hennen, R. A. Villafuerte, M. L. Butman, P. Tran, L. T. Kerner, B. Cohen, P. F. Renshaw, A comparison of brain and serum pharmacokinetics of *R*-fluoxetine and racemic fluoxetine: A 19-F MRS study. *Neuropsychopharmacology* **30**, 1576–1583 (2005). Medline doi:10.1038/sj.npp.1300749

8. E. Honoré, The neuronal background K_{2P} channels: Focus on TREK1. *Nat. Rev. Neurosci.* **8**, 251–261 (2007). Medline doi:10.1038/nrn2117

9. A. Gurney, B. Manoury, Two-pore potassium channels in the cardiovascular system. *Eur. Biophys. J.* **38**, 305–318 (2009). Medline doi:10.1007/s00249-008-0326-8

10. S. G. Brohawn, E. B. Campbell, R. MacKinnon, Domain-swapped chain connectivity and gated membrane access in a Fab-mediated crystal of the human TRAAK K^+ channel. *Proc. Natl. Acad. Sci. U.S.A.* **110**, 2129–2134 (2013). Medline doi:10.1073/pnas.1218950110

11. S. G. Brohawn, J. del Mármol, R. MacKinnon, Crystal structure of the human K2P TRAAK, a lipid- and mechano-sensitive K^+ ion channel. *Science* **335**, 436–441 (2012). Medline doi:10.1126/science.1213808

12. A. N. Miller, S. B. Long, Crystal structure of the human two-pore domain potassium channel K2P1. *Science* **335**, 432–436 (2012). Medline doi:10.1126/science.1213274

13. S. N. Bagriantsev, R. Peyronnet, K. A. Clark, E. Honoré, D. L. Minor Jr., Multiple modalities converge on a common gate to control K_{2P} channel function. *EMBO J.* **30**, 3594–3606 (2011). Medline doi:10.1038/emboj.2011.230

14. P. L. Piechotta, M. Rapedius, P. J. Stansfeld, M. K. Bollepalli, G. Ehrlich, I. Andres-Enguix, H. Fritzenschaft, N. Decher, M. S. Sansom, S. J. Tucker, T. Baukrowitz, The pore structure and gating mechanism of K2P channels. *EMBO J.* **30**, 3607–3619 (2011). Medline doi:10.1038/emboj.2011.268

15. Materials and methods are available as supplementary materials on *Science* Online.

16. S. G. Brohawn, E. B. Campbell, R. MacKinnon, Physical mechanism for gating and mechanosensitivity of the human TRAAK K^+ channel. *Nature* **516**, 126–130 (2014). Medline doi:10.1038/nature14013

17. M. Lolicato, P. M. Riegelhaupt, C. Arrigoni, K. A. Clark, D. L. Minor Jr., Transmembrane helix straightening and buckling underlies activation of mechanosensitive and thermosensitive K_{2P} channels. *Neuron* **84**, 1198–1212 (2014). Medline doi:10.1016/j.neuron.2014.11.017

18. M. Zhou, J. H. Morais-Cabral, S. Mann, R. MacKinnon, Potassium channel receptor site for the inactivation gate and quaternary amine inhibitors. *Nature* **411**, 657–661 (2001). Medline doi:10.1038/35079500

19. D. A. Köpfer, C. Song, T. Gruene, G. M. Sheldrick, U. Zachariae, B. L. de Groot, Ion permeation in K^+ channels occurs by direct Coulomb knock-on. *Science* **346**, 352–355 (2014). Medline doi:10.1126/science.1254840

20. Single-letter abbreviations for the amino acid residues are as follows: A, Ala; C, Cys; D, Asp; E, Glu; F, Phe; G, Gly; H, His; I, Ile; K, Lys; L, Leu; M, Met; N, Asn; P, Pro; Q, Gln; R, Arg; S, Ser; T, Thr; V, Val; W, Trp; and Y, Tyr.

21. E. Honoré, F. Maingret, M. Lazdunski, A. J. Patel, An intracellular proton sensor commands lipid- and mechano-gating of the K^+ channel TREK-1. *EMBO J.* **21**, 2968–2976 (2002). Medline doi:10.1093/emboj/cdf288

22. F. Maingret, A. J. Patel, F. Lesage, M. Lazdunski, E. Honoré, Mechano- or acid stimulation, two interactive modes of activation of the TREK-1 potassium channel. *J. Biol. Chem.* **274**, 26691–26696 (1999). Medline doi:10.1074/jbc.274.38.26691

23. S. N. Bagriantsev, K. A. Clark, D. L. Minor Jr., Metabolic and thermal stimuli control K_{2P}2.1 (TREK-1) through modular sensory and gating domains. *EMBO J.* **31**, 3297–3308 (2012). Medline doi:10.1038/emboj.2012.171

24. J. Chemin, A. J. Patel, F. Duprat, F. Sachs, M. Lazdunski, E. Honore, Up- and down-regulation of the mechano-gated K_{2P} channel TREK-1 by PIP_2 and other membrane phospholipids. *Pflugers Arch.* **455**, 97–103 (2007). Medline doi:10.1007/s00424-007-0250-2

25. G. Sandoz, D. Douguet, F. Chatelain, M. Lazdunski, F. Lesage, Extracellular acidification exerts opposite actions on TREK1 and TREK2 potassium channels via a single conserved histidine residue. *Proc. Natl. Acad. Sci. U.S.A.* **106**, 14628–14633 (2009). Medline doi:10.1073/pnas.0906267106

26. A. Anishkin, S. H. Loukin, J. Teng, C. Kung, Feeling the hidden mechanical forces in lipid bilayer is an original sense. *Proc. Natl. Acad. Sci. U.S.A.* **111**, 7898–7905 (2014). Medline doi:10.1073/pnas.1313364111

27. S. G. Brohawn, Z. Su, R. MacKinnon, Mechanosensitivity is mediated directly by the lipid membrane in TRAAK and TREK1 K^+ channels. *Proc. Natl. Acad. Sci. U.S.A.* **111**, 3614–3619 (2014). Medline doi:10.1073/pnas.1320768111

28. J. Teng, S. Loukin, A. Anishkin, C. Kung, The force-from-lipid (FFL) principle of mechanosensitivity, at large and in elements. *Pflugers Arch.* **467**, 27–37 (2015). Medline doi:10.1007/s00424-014-1530-2

29. P. Aryal, F. Abd-Wahab, G. Bucci, M. S. Sansom, S. J. Tucker, A hydrophobic barrier deep within the inner pore of the TWIK-1 K2P potassium channel. *Nat. Commun.* **5**, 4377 (2014). Medline doi:10.1038/ncomms5377

30. P. Aryal, F. Abd-Wahab, G. Bucci, M. S. Sansom, S. J. Tucker, Influence of lipids on the hydrophobic barrier within the pore of the TWIK-1 K2P channel. *Channels* **9**, 44–49 (2015). Medline

31. S. Newstead, S. Ferrandon, S. Iwata, Rationalizing α-helical membrane protein crystallization. *Protein Sci.* **17**, 466–472 (2008). Medline doi:10.1110/ps.073263108

32. J. L. Parker, S. Newstead, Current trends in α-helical membrane protein crystallization: An update. *Protein Sci.* **21**, 1358–1365 (2012). Medline doi:10.1002/pro.2122

33. T. M. Koenig, D. Mitchell, A convenient method for preparing enantiomerically pure norfluoxetine, fluoxetine and tomoxetine. *Tetrahedron Lett.* **35**, 1339–1342 (1994). doi:10.1016/S0040-4039(00)76212-5

34. W. Kabsch, *XDS*. *Acta Crystallogr. D* **66**, 125–132 (2010). Medline doi:10.1107/S0907444909047337

35. P. Evans, Scaling and assessment of data quality. *Acta Crystallogr. D* **62**, 72–82 (2006). Medline doi:10.1107/S0907444905036693

36. A. J. McCoy, R. W. Grosse-Kunstleve, P. D. Adams, M. D. Winn, L. C. Storoni, R. J. Read, Phaser crystallographic software. *J. Appl. Crystallogr.* **40**, 658–674 (2007). Medline doi:10.1107/S0021889807021206

37. P. Emsley, B. Lohkamp, W. G. Scott, K. Cowtan, Features and development of *Coot*. *Acta Crystallogr. D* **66**, 486–501 (2010). Medline doi:10.1107/S0907444910007493

38. P. D. Adams, P. V. Afonine, G. Bunkóczi, V. B. Chen, I. W. Davis, N. Echols, J. J. Headd, L. W. Hung, G. J. Kapral, R. W. Grosse-Kunstleve, A. J. McCoy, N. W. Moriarty, R. Oeffner, R. J. Read, D. C. Richardson, J. S. Richardson, T. C. Terwilliger, P. H. Zwart, *PHENIX*: A comprehensive Python-based system for macromolecular structure solution. *Acta Crystallogr. D* **66**, 213–221 (2010). Medline doi:10.1107/S0907444909052925

39. G. Bricogne, E. Blanc, M. Brandl, C. Flensburg, P. Keller, W. Paciorek, P. Roversi, A. Sharff, O. S. Smart, C. Vonrhein, T. O. Womack, BUSTER, versions 2.10.1 and 2.11.2 (Global Phasing Ltd, Cambridge, 2011).

40. V. B. Chen, W. B. Arendall III, J. J. Headd, D. A. Keedy, R. M. Immormino, G. J. Kapral, L. W. Murray, J. S. Richardson, D. C. Richardson, *MolProbity*: All-atom structure validation for macromolecular crystallography. *Acta Crystallogr. D* **66**, 12–21 (2010). Medline doi:10.1107/S0907444909042073

41. E. G. Hutchinson, J. M. Thornton, PROMOTIF—A program to identify and analyze structural motifs in proteins. *Protein Sci.* **5**, 212–220 (1996). Medline doi:10.1002/pro.5560050204

42. The PyMol Molecular Graphics System, version 1.5.0.4 (Schrodinger, LLC, 2010); www.pymol.org.

43. E. F. Pettersen, T. D. Goddard, C. C. Huang, G. S. Couch, D. M. Greenblatt, E. C. Meng, T. E. Ferrin, UCSF Chimera—A visualization system for exploratory research and analysis. *J. Comput. Chem.* **25**, 1605–1612 (2004). Medline doi:10.1002/jcc.20084

44. A. Šali, T. L. Blundell, Comparative protein modelling by satisfaction of spatial restraints. *J. Mol. Biol.* **234**, 779–815 (1993). Medline doi:10.1006/jmbi.1993.1626

45. P. J. Bond, M. S. Sansom, Insertion and assembly of membrane proteins via simulation. *J. Am. Chem. Soc.* **128**, 2697–2704 (2006). Medline doi:10.1021/ja0569104

46. C. Oostenbrink, A. Villa, A. E. Mark, W. F. van Gunsteren, A biomolecular force field based on the free enthalpy of hydration and solvation: The GROMOS force-field parameter sets 53A5 and 53A6. *J. Comput. Chem.* **25**, 1656–1676 (2004). Medline doi:10.1002/jcc.20090

47. E. L. Veale, E. Al-Moubarak, N. Bajaria, K. Omoto, L. Cao, S. J. Tucker, E. B. Stevens, A. Mathie, Influence of the N terminus on the biophysical properties and pharmacology of TREK1 potassium channels. *Mol. Pharmacol.* **85**, 671–681 (2014). Medline doi:10.1124/mol.113.091199

48. O. S. Smart, J. G. Neduvelil, X. Wang, B. A. Wallace, M. S. Sansom, HOLE: A program for the analysis of the pore dimensions of ion channel structural models. *J. Mol. Graph.* **14**, 354–360, 376 (1996). Medline doi:10.1016/S0263-7855(97)00009-X

49. E. Krissinel, K. Henrick, Inference of macromolecular assemblies from crystalline state. *J. Mol. Biol.* **372**, 774–797 (2007). Medline doi:10.1016/j.jmb.2007.05.022